2011

# Vertical structure, seasonal drawdown, and net community production in the Ross Sea, Antarctica

Matthew C. Long
*Stanford University*

Robert B. Dunbar
*Stanford University*

Philippe D. Tortell
*University of British Columbia*

Walker O. Smith Jr.
*Virginia Institute of Marine Science*, wos@vims.edu

David A. Mucciarone
*Stanford University*

*See next page for additional authors*

# Vertical structure, seasonal drawdown, and net community production in the Ross Sea, Antarctica

Matthew C. Long,[1,2] Robert B. Dunbar,[1] Philippe D. Tortell,[3] Walker O. Smith,[4] David A. Mucciarone,[1] and Giacomo R. DiTullio[5]

Received 13 November 2009; revised 11 April 2011; accepted 29 July 2011; published 21 October 2011.

[1] We calculate net community production (NCP) during summer 2005–2006 and spring 2006 in the Ross Sea using multiple approaches to determine the magnitude and consistency of rates. Water column carbon and nutrient inventories and surface ocean $O_2$/Ar data are compared to satellite-derived primary productivity (PP) estimates and $^{14}C$ uptake experiments. In spring, NCP was related to stratification proximal to upper ocean fronts. In summer, the most intense C drawdown was in shallow mixed layers affected by ice melt; depth-integrated C drawdown, however, increased with mixing depth. $\Delta O_2$/Ar-based methods, relying on gas exchange reconstructions, underestimate NCP due to seasonal variations in surface $\Delta O_2$/Ar and NCP rates. Mixed layer $\Delta O_2$/Ar requires approximately 60 days to reach steady state, starting from early spring. Additionally, cold temperatures prolong the sensitivity of gas exchange reconstructions to past NCP variability. Complex vertical structure, in addition to the seasonal cycle, affects interpretations of surface-based observations, including those made from satellites. During both spring and summer, substantial fractions of NCP were below the mixed layer. Satellite-derived estimates tended to overestimate PP relative to $^{14}C$-based estimates, most severely in locations of stronger upper water column stratification. Biases notwithstanding, NCP-PP comparisons indicated that community respiration was of similar magnitude to NCP. We observed that a substantial portion of NCP remained as suspended particulate matter in the upper water column, demonstrating a lag between production and export. Resolving the dynamic physical processes that structure variance in NCP and its fate will enhance the understanding of the carbon cycling in highly productive Antarctic environments.

**Citation:** Long, M. C., R. B. Dunbar, P. D. Tortell, W. O. Smith, D. A. Mucciarone, and G. R. DiTullio (2011), Vertical structure, seasonal drawdown, and net community production in the Ross Sea, Antarctica, *J. Geophys. Res.*, *116*, C10029, doi:10.1029/2009JC005954.

## 1. Introduction

[2] Net community production (NCP), defined as net primary production (NPP) minus heterotrophic respiration, is the maximum amount of organic material that is available for export from the surface to the deep sea. In this sense, NCP is a good metric of biological activity's net effect on carbon cycling in the upper ocean. Antarctic bottom water (AABW) formation regions play an important role in the global carbon cycle [*Sarmiento et al.*, 2004; *Marinov et al.*, 2006]. Water from these regions sinks into the ocean interior and is thereby removed from contact with the atmosphere for 100's of years. This feature of thermohaline circulation means that long-term, atmosphere-ocean partitioning of $CO_2$ is sensitive to processes affecting the composition of AABW [*Ito and Follows*, 2005]. Surface ocean primary productivity (PP) along the Antarctic margin modulates the carbon content of AABW by consuming nutrients and converting dissolved inorganic carbon (DIC) into sinking organic material. This process also lowers the partial pressure of $CO_2$ in the surface ocean, important for maintaining a positive gas-exchange gradient [*Sweeney*, 2003; *Arrigo et al.*, 2008a]. While it has been documented that NCP in AABW regions exerts an important control on the global carbon cycle, including over glacial/interglacial timescales [*Sigman and Boyle*, 2000], the modern variability of NCP in these regions remains poorly quantified due to high spatial and temporal variability, difficulties associated with experimental determination of NCP/NPP rates, and the remoteness of these areas.

[3] The Ross Sea is situated over a broad continental shelf along the Antarctic margin and is an important site of deep-water formation [*Orsi et al.*, 2002]. Observations and models

[1]Environmental Earth System Science, Stanford University, Stanford, California, USA.
[2]Now at National Center for Atmospheric Research, Boulder, Colorado, USA.
[3]Department of Earth and Ocean Sciences and Department of Botany, University of British Columbia, Vancouver, British Columbia, Canada.
[4]Virginia Institute of Marine Science, College of William and Mary, Gloucester Point, Virginia, USA.
[5]Grice Marine Laboratory, College of Charleston, Charleston, South Carolina, USA.


0148-0227/11/2009JC005954

of the Ross Sea continental shelf suggest it is an important sink for anthropogenic $CO_2$ [*Arrigo et al.*, 2008a; *Sandrini et al.*, 2007]. The dynamics of this sink are closely coupled to the annual cycle of sea ice and NCP in the region [*Sweeney*, 2003]. Ross Sea surface waters are ice covered most of the year. Each spring, however, usually beginning in about late-October through mid-November, sea ice clears over the continental shelf, exposing surface water to the atmosphere for three to four months of the austral summer. This annual expansion of the Ross Sea 'polynya' provides an opportunity for large-scale exchange of gases, heat and momentum between the ocean and atmosphere.

[4] The annual expansion of the Ross Sea polynya coincides with the development of a large phytoplankton bloom, dominated by two algal groups: the haptophyte *Phaeocystis antarctica* and several diatom species [*DiTullio and Smith*, 1996; *Arrigo et al.*, 1999; *Arrigo and van Dijken*, 2004]. Typically, *P. antarctica* becomes established early in the season, when substantial sea ice is still present, and dominates the relatively unstratified waters of the central polynya [*Arrigo et al.*, 1998b]. Diatoms bloom later in the season, concentrated in a semi-distinct pelagic habitat along the western continental margin, including Terra Nova Bay, where sea-ice-derived freshwater stabilizes the water column, causing mixed layer depths (MLDs) to shoal [*Arrigo et al.*, 2003]. As summer progresses, accumulation of dissolved oxygen and drawdown of DIC and nutrients are evident in the surface waters [*Bates et al.*, 1998; *Bender et al.*, 2000; *Sweeney et al.*, 2000; *Arrigo et al.*, 1999; *Dunbar et al.*, 2003]. Cooling, sea ice formation, deep convection and wind mixing work to re-homogenize the water column during autumn and winter [*Gordon et al.*, 2000]. These processes erode the vertical gradients that developed over summer, thus leaving the water column following winter relatively homogenous.

[5] As is typical of the Southern Ocean, macronutrients (nitrate, phosphate, and silica) are generally replete in Ross Sea surface waters year-round. High concentrations of surface nutrients, sufficient trace metal supply [*Fitzwater et al.*, 2000; *Sedwick et al.*, 2000], and incipient stratification drive high rates of primary productivity (e.g., >200 mmol C $m^{-2}$ $d^{-1}$) in early spring [*Smith et al.*, 2000; *Arrigo and van Dijken*, 2004]. In the central Ross Sea, NPP typically peaks in late-December, early-January, and subsequently declines through February into March [*Smith et al.*, 2000; *Arrigo and van Dijken*, 2004]. Since macronutrients are rarely drawn down below growth-limiting concentrations, it is generally believed that the Ross Sea bloom terminates due to iron limitation [*Tagliabue and Arrigo*, 2005; *Sedwick et al.*, 2000; *Smith et al.*, 2000; *Arrigo et al.*, 2003].

[6] Given its central role in the global carbon cycle and its likely sensitivity to climate, regular and accurate measurement of NCP is important to understand global carbon cycling and diagnose potential climate-carbon feedbacks [*Sarmiento et al.*, 1998]. Unfortunately, NPP and NCP are highly dynamic, displaying significant variability on both short time and length scales. Previous studies, using a variety of approaches, have estimated the mean annual NCP over the Ross Sea continental shelf to range from about 4–10 mol C $m^{-2}$ [*Bates et al.*, 1998; *Smith and Gordon*, 1997; *Sweeney et al.*, 2000]. A satellite algorithm tuned to the region estimates that net annual carbon fixation (1996–2006) over the Ross Sea continental shelf ranged between about 3 and 35 Tg C, with mean NPP of about 15 mol C $m^{-2}$ [*Arrigo et al.*, 2008b]. In the Ross Sea, interannual variability in NPP has been linked to differing sea ice conditions and atmospheric forcing driving seasonally variable MLDs [*Sweeney et al.*, 2000; *Arrigo et al.*, 1998b; *Arrigo and van Dijken*, 2003]. Large-scale surface gradients in Ross Sea NPP/NCP align with taxonomic distributions linked to sea ice conditions and stratification [*Sweeney et al.*, 2000]. In addition to these broad gradients, meso- and submesoscale variability is significant in the Ross Sea [*Hales and Takahashi*, 2004], a result of biological rate processes entrained with a constantly changing geophysical fluid.

[7] In addition to the highly dynamic nature of NPP/NCP, methodological issues associated with experimental determination are significant. One commonly employed approach to measure NPP is $^{14}C$ incubations. In addition to potential artifacts associated with containment and manipulation of a natural community, the degree to which label uptake reflects the balance of production and various respiration pathways is somewhat ambiguous and highly dependent on incubation timescales [*Marra*, 2002]. Ideally, rates of NPP/NCP should be determined in situ, using geochemical techniques. This approach has the advantage of addressing rates in the natural setting, but requires assumptions regarding physically and biologically mediated fluxes to perform mass balance calculations. Even when assumptions are tenable, in situ measurements are labor intensive and constrained in time and space.

[8] Given the patchiness inherent in oceanic biological fields [*Doney et al.*, 2003], robust measures of areally-integrated rates are challenging to develop from discrete point measurements. Satellite methods provide information on synoptic scales; however, satellite-based NPP estimates invoke models that generalize relationships between measured variables (surface ocean color, sea surface temperature, and solar radiation) and depth integrated NPP estimates [*Behrenfeld and Falkowski*, 1997]. These algorithms require regional calibration, which has proved problematic in the Southern Ocean [*Carr et al.*, 2006]. Moreover, satellite-based NPP estimates do not provide direct information on NCP, a more geochemically relevant quantity. The conversion of satellite NPP estimates to export flux, a quantity equivalent to NCP in steady state, requires algorithms that incorporate additional uncertainty [*Laws*, 1991; *Laws et al.*, 2000; *Dunne et al.*, 2007; *Lutz et al.*, 2007].

[9] In this study, we calculate NCP during summer 2005–2006 and spring 2006–2007 in the Ross Sea. Our primary objective is to use multiple tracers of productivity to determine the magnitude and consistency of NCP rates. We compare geochemical measurements of NCP with operational means of assessing NPP: $^{14}C$-incubations and a satellite primary productivity algorithm tuned to the region. Additionally, we evaluate the capacity for inferring NCP from surface measurements of dissolved oxygen saturation normalized to argon ($\Delta O_2/Ar$): this quantity can be interpreted as biologically-induced oxygen saturation. New mass spectrometric techniques are increasingly being deployed as a means of examining biologically-induced oxygen variability at high spatial resolution, over large distances [*Tortell*, 2005; *Kaiser et al.*, 2005; *Guéguen and Tortell*, 2008; *Tortell and Long*, 2009; *Cassar et al.*, 2009]. Several studies have used

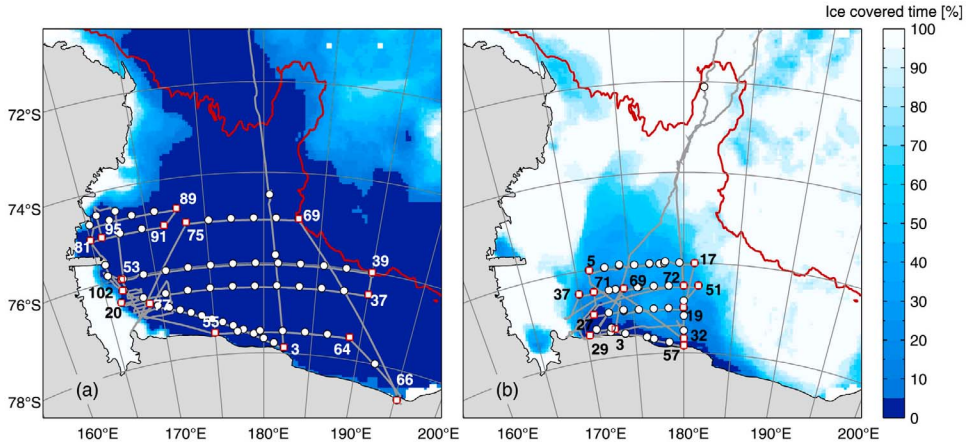


**Figure 1.** Cruise track (light gray line) and CTD station locations (white symbols) for (a) CORSACS-I (C1, NBP06-01) and (b) CORSACS-II (C2, NBP06-08). Color shows the percentage of the time during the cruise that a region was ice covered, based on the polynya signature simulation method (PSSM) [*Markus and Burns*, 1995]. Dark red line is the 1000 m isobath. Red squares highlight labeled stations.

surface biological oxygen saturation measurements to develop estimates of Southern Ocean NCP [*Hendricks et al.*, 2004; *Cassar et al.*, 2007; *Reuer et al.*, 2007; *Tortell and Long*, 2009]. The computational approach employed to relate surface $\Delta O_2/Ar$ to NCP relies on the assumption that $O_2$ in the mixed layer is at steady state [*Kaiser et al.*, 2005; *Reuer et al.*, 2007]. This has constrained the focus of these studies to Southern Ocean regions north of the seasonal ice zone. South of the sea ice zone, this assumption is more tenuous, and mixed layer mass balances are further complicated by weak vertical stratification. We diagnose the degree to which the assumptions invoked in $\Delta O_2/Ar$-based NCP calculations influence productivity estimates for the Ross Sea region.

[10] Our study is unique in that we combine high-resolution surface gas measurements with vertically resolved data. While numerous studies have applied tracer budgets or examined satellite- or incubation-derived primary productivity estimates, seldom have inter-comparisons between in situ methods been applied. Our analysis permits evaluation of the assumptions implicit in various methods and provides context over a range of spatial and temporal scales.

## 2. Methods

### 2.1. Oceanographic Cruises

[11] As part of the CORSACS (Controls on Ross Sea Algal Community Structure) program, we conducted two expeditions to the Ross Sea during 2005 and 2006 aboard the R/V *Nathaniel B. Palmer*. The first cruise, NBP06-01 (December 2005 to January 2006; hereafter referred to as C1), sampled conditions representative of summer within the polynya. The second cruise, NBP06-08 (November–December 2006; hereafter referred to as C2), sampled spring conditions during the initiation of the bloom. Figure 1 shows station locations for both cruises, as well as ice coverage, computed using the polynya signature simulation method (PSSM) [*Markus and Burns*, 1995]. As observed in previous studies [*DiTullio and Smith*, 1996; *Arrigo et al.*, 1998b], phytoplankton assemblages were dominated by *Phaeocystis antarctica* during the early spring bloom, and by a mixture of diatoms and *P. antarctica* during the later summer.

### 2.2. Analytical Methods

#### 2.2.1. CTD Casts and Sample Collection

[12] Discrete water column samples were collected using 10 L Niskin bottles mounted on an epoxy-coated 24-bottle rosette, equipped with a SeaBird Electronics (SBE) Model SBE-911+ conductivity, temperature, and depth (CTD) sensor. Water samples were drawn in accord with JGOFS protocols [*Knap et al.*, 1994]. Post-processed data and description of analytical methods is archived at the Biological and Chemical Oceanography Data Management Office (http://osprey.bcodmo.org/project.cfm?flag=view&id=40&sortby=project) and at Stanford University (ftp://pangea.stanford.edu/pub/dunbar/CORSACSHydrographyReports/). Below we report a brief overview of our analytical methods.

#### 2.2.2. Salinity, Oxygen, Nutrients and Chlorophyll *a*

[13] Salinity samples were analyzed at 24°C using a Guildline 8400 Autosal four-electrode salinometer at sea. Autosal bottle salinity values were used to assess the performance of both CTD conductivity cells and correct for sensor drift.

[14] Discrete dissolved oxygen measurements were made with a Lamont-Doherty Earth Observatory amperometric oxygen titration system [*Culberson and Huang*, 1987]. Based on standards and replicate analyses, analytical precision was ±0.01mL $L^{-1}$. Several discrete samples for each cast were used to calibrate the CTD oxygen sensor.

[15] A Lachat Quickchem FIA+ series 8000 was used for automated analysis of $NH_4^+ + NO_3^- + NO_2^-$, $SiO_2$, and $PO_4^{3-}$ following the methodology of *Gordon et al.* [1993]. The nutrient measurements had a precision of approximately ±1% based on replicate analysis.

[16] Chlorophyll *a* concentrations were determined by HPLC analyses using the protocol described by *DiTullio and Geesey* [2002].

#### 2.2.3. Carbon

[17] Samples for dissolved inorganic carbon (DIC) analysis were collected following *Dickson and Goyet* [1994]. DIC was

measured by infrared absorption analysis of $CO_2$ evolved from acidified samples in a nitrogen carrier gas stream, using a custom-built automated injection system connected to an infrared gas analyzer (LI-COR LI7000). The injection system consists of a high-precision digital pump (Kloehn Versa-Pump 6), which delivers a precise volume of seawater to a small sparging tube; 0.1 mL of phosphoric acid (3 N) is added by a micro-pump and the sample bubbled with ultrahigh purity nitrogen equipped with an in-line $CO_2$ scrubber. Before entering the LI-COR, the gas stream passes through a nafion dryer and a magnesium perchlorate water trap. The gas flow is regulated using a silicon orifice mass flow controller (Redwood Microsystems, MEMS-Flow Model 9900).

[18] Integrating the infrared absorbance signal with respect to time yields the total amount of $CO_2$ evolved from the sample. These peak-area measurements were calibrated using certified reference materials (CRM; http://andrew.ucsd.edu/co2qc). Samples were run in batches of 12; CRM standards were run between every 4–6 unknowns to correct for instrument drift (generally <0.06%) due to moisture accumulation over the course of a run. Precision estimated on the basis of triplicate analysis of all (>4000) unknown seawater samples was ±1.2 $\mu$mol kg$^{-1}$.

[19] Surface $pCO_2$ measurements were made using the LDEO underway system for surface water $pCO_2$ measurements installed on the NBP [*Newberger*, 2004]. Details of the system can found at (http://www.ldeo.columbia.edu/res/pi/CO2/).

[20] Particulate organic carbon (POC) and nitrogen (PON) were measured following [*Knap et al.*, 1994]. Particulate matter was collected by filtering 2 to 12 liters of seawater through precombusted Whatman GFC filters. These were rinsed with 10 mL of 0.01 N HCl immediately after filtration, air-dried, and returned to Stanford University for analysis using a Carlo Erba NA1500 elemental analyzer/Conflo II device and a Finnigan Delta Plus mass spectrometer.

#### 2.2.4. Membrane Inlet Mass Spectrometry

[21] Dissolved gas analysis was conducted using membrane inlet mass spectrometry (MIMS) as described by *Guéguen and Tortell* [2008]. During underway analysis, concentrations of $CO_2$, dimethyl sulfide (DMS) and $\Delta O_2$/Ar ratios (see below) were measured every ~30 seconds, corresponding to a mean spatial resolution of ~50 to 300 m depending upon the ship's speed. Raw ion currents were calibrated to yield concentrations as described by *Guéguen and Tortell* [2008].

### 2.3. Stratification Metrics

[22] We diagnosed the MLD as the point in the water column where the density exceeds the surface density by some incremental difference $\Delta\sigma_t$ ($\sigma_t = \rho - 1000$ kg m$^{-3}$). The choice of $\Delta\sigma_t$ is somewhat arbitrary and we consider a range of values that have been used in previous studies, from $\Delta\sigma_t$ = 0.02 to 0.125. In addition to MLD, we make use of the Brunt-Väisälä or buoyancy frequency ($N^2 = -(g/\rho)d\rho/dz$), which provides a measure of the strength of stratification.

### 2.4. Net Primary and Net Community Production

[23] We examined depth-integrated distributions of $O_2$, DIC, and total inorganic nitrogen (TIN = $NO_3^- + NO_2^- + NH^+$) as measures of biological productivity in the mixed layer (ML). Conceptually, the time rate of change of one of these tracers in the ocean surface, arbitrarily referred to as $M$, can be represented as a function of biologically- and physically-mediated fluxes. Ignoring advective and diffusive fluxes and defining the vertical boundary of a control volume at depth $h$, the basic mass balance equation is

$$h\frac{\partial_M}{\partial t} = P_M - R_M - F_M \quad (1)$$

where $P_M$ is net autotrophic production (or consumption) of $M$, $R_M$ represents metabolic release (or consumption) of $M$ due to community respiration, and $F_M$ is the flux across the sea-air interface, defined here such that negative values indicate a flux into the ocean. NCP is the balance of net primary production and community respiration (NCP = $P_M - R_M$) [*Bender et al.*, 1987].

[24] Equation (1) does not account for freshwater fluxes associated with ice formation and melting, which can substantially concentrate or dilute dissolved constituents. We normalize DIC and TIN to a salinity of 34.5, approximately the mean salinity of the entire Ross Seawater column. Salinity normalized quantities are denoted with a small '*s*' (i.e., *s*DIC or *s*TIN).

[25] Carbon drawdown is assumed to occur in consistent stoichiometric proportion to oxygen and nitrogen drawdown. To convert between nitrogen and carbon deficits, we use the average C:N drawdown stoichiometry for the Ross Sea polynya determined by *Arrigo et al.* [2002] and *Dunbar et al.* [2003] (C:N = 7.23 ± 0.03). There is a two-fold difference in C:P stoichiometry between *P. antarctica* and diatoms, which complicates the spatial structure of $PO_4^{3-}$ [*Arrigo et al.*, 2002; *Dunbar et al.*, 2003]. To convert between oxygen and carbon, we use the global mean remineralization ratios of *Anderson and Sarmiento* [1994] ($-O_2$:C = 170:117). Note that *Anderson and Sarmiento* [1994] use a C:N ratio of 7.31.

#### 2.4.1. Deficit Integrals

[26] Given an initial water column profile and excluding gas exchange, the depth integrated drawdown or 'deficit integral' of a tracer ($M$; units of concentration) above depth $h$ can be computed as

$$\int_0^h \delta M\, dz = -\int_0^h \left(M_f - M_0\right) dz \quad (2)$$

where $M_0$ is the initial condition at the beginning of the season and $M_f$ is the distribution at the time of measurement. We use the symbol '$\delta$' to denote the change in $M$ due to biological removal (input) of a tracer from (to) the surface ocean. The minus sign reflects a convention that positive rates of NCP yield positive deficit integrals, i.e., $M_f < M_0$ due to biological consumption of $M$.

[27] During spring and summer in the Ross Sea, surface water properties change rapidly, while deep water changes more slowly. Since the water column experiences an annual "reset" due to winter deep convection, the initial profile is reasonably well constrained by measurements of deep continental shelf water characteristics (below 200 m); we use these deep water measurements as a proxy for winter surface water conditions [*Gordon et al.*, 2000; *Sweeney et al.*, 2000].

[28] Oxygen and $CO_2$ exchange with the atmosphere over the course of the season will affect the deficit integrals. Gas exchange is a minor term (<10%) relative to seasonal DIC

drawdown [*Sweeney et al.*, 2000]. Seasonal NCP on the basis of $\delta s$DIC then is

$$\mathrm{NCP}_h = \int_0^h \delta s\mathrm{DIC}\, dz - \int_0^f F_{\mathrm{co}_2} dt \tag{3}$$

where $\mathrm{NCP}_h$ refers to NCP above depth $h$.

[29] Sea-air flux of $CO_2$ is computed as

$$F_{\mathrm{co}_2} = (1-A)k^{\mathrm{co}_2}\gamma\left(p\mathrm{CO}_2^{sw} - p\mathrm{CO}_2^{atm}\right) \tag{4}$$

where $A$ is the ice fractional ice coverage, $\gamma$ is the temperature and salinity dependent solubility of $CO_2$ [*Weiss*, 1974], and $k^{\mathrm{co}_2}$ is the gas transfer velocity (m $d^{-1}$), calculated as a function of wind speed and the temperature-dependent Schmidt number [*Wanninkhof*, 1992].

[30] To compute time-integrated sea-air $CO_2$ flux, we use *GLOBALVIEW-CO*$_2$ [2008] to estimate $p\mathrm{CO}_2^{atm}$. To estimate the time evolution of $p\mathrm{CO}_2^{sw}$ prior to our arrival on site, we assume a linear decline over the growing season from 425 $\mu$atm [*Sweeney*, 2003], to the measured partial pressure. While $p\mathrm{CO}_2$ does not change linearly with constant NCP, we do not know the time-varying nature of past production, thus we use the assumption of linearity to avoid other ad hoc inferences. To estimate time variations in $\gamma$, we use weekly sea surface temperature data at 1° × 1° from the Reynolds Optimally Interpolated Sea Surface Temperature product (ROISST) [*Reynolds et al.*, 2002]. SSM/I ice concentration data [*Cavalieri et al.*, 1990] and NCEP-NCAR daily wind data (http://www.esrl.noaa.gov/psd/data/gridded/reanalysis/) [*Kalnay et al.*, 1996] are used to force the sea-air flux computation. Using this approach, we calculate time-integrated gas flux at each station ignoring the effect of lateral advection. We assume that seasonal drawdown begins on 1 November, which, based on an examination of satellite sea ice data, is prior to substantial clearing of sea ice.

[31] In addition to gas exchange, $s$DIC is sensitive to calcium carbonate ($CO_3^{2-}$) precipitation and dissolution. The presence of pteropods in Ross Sea sediment traps indicates the potential for biological $CO_3^{2-}$ precipitation to contribute to spatial and interannual variability in the surface distribution of alkalinity (*Alk*) [*Dunbar*, 1984; *Collier et al.*, 2000]. Others have found, however, that surface *Alk* variability is small (~5%) relative to $s$DIC drawdown [*Bates et al.*, 1998; *Sweeney et al.*, 2000]; thus, following *Sweeney et al.* [2000], we neglect the effect of *Alk* on the overall carbon mass balance.

#### 2.4.2. Surface $O_2$ Measurements

[32] Oxygen is considerably less soluble in seawater than $CO_2$. As a result, gas exchange timescales are considerably shorter for $O_2$ and mechanical processes, such as bubble dynamics caused by breaking waves, are of much greater importance. Surface measurements of $O_2$/Ar ratios, however, can be used to reconstruct biological $O_2$ fluxes since Ar is a physical analog for $O_2$, with virtually identical solubility properties [*Craig and Hayward*, 1987]. Biological oxygen saturation is defined as

$$\Delta\mathrm{O}_2/\mathrm{Ar} = \frac{(\mathrm{O}_2/\mathrm{Ar})_{sw}}{(\mathrm{O}_2/\mathrm{Ar})_{sat}} - 1 \tag{5}$$

where $(O_2/Ar)_{sw}$ is the measured concentration ratio and $(O_2/Ar)_{sat}$ is the saturation concentration ratio, given as a function of temperature and salinity by the solubility equations of *García and Gordon* [1992] and *Hamme and Emerson* [2004].

[33] To develop estimates of NCP, surface $\Delta O_2$/Ar measurements are interpreted to reflect water column concentrations to the depth of the ML [e.g., *Kaiser et al.*, 2005; *Reuer et al.*, 2007; *Tortell and Long*, 2009]. In order to move from a concentration measurement to a biological rate, it is necessary to account for the effect of physically mediated fluxes across ML boundaries. If advective and diffusive fluxes are neglected, the only remaining boundary is the sea-air interface and the biological oxygen ML mass balance is simply

$$\frac{\partial \mathrm{O}_2}{\partial t} = \mathrm{NCP} - (1-A)k^{\mathrm{o}_2}(\Delta\mathrm{O}_2/\mathrm{Ar})\mathrm{O}_{2,sat} \tag{6}$$

where $k^{\mathrm{O}_2}$ is the piston velocity and $O_{2,sat}$ is the temperature and salinity dependent $O_2$ saturation concentration [*Kaiser et al.*, 2005]. In steady state, then

$$\mathrm{NCP} = (1-A)k^{\mathrm{o}_2}(\Delta\mathrm{O}_2/\mathrm{Ar})\mathrm{O}_{2,sat} \tag{7}$$

On this basis, NCP is computed by reconstructing sea-air flux from the wind history [*Juranek and Quay*, 2005; *Kaiser et al.*, 2005; *Reuer et al.*, 2007].

[34] *Reuer et al.* [2007] present a scheme to estimate an effective piston velocity ($k^{\mathrm{O}_2}$) that is a weighted average computed from daily wind speeds extending 60–120 days prior to the day of sampling. We will refer to this method as the "weighted piston velocity" (WPV) method. This method yields weighting factors that place greater emphasis on recent wind history and diminished emphasis on days preceding a large wind event.

### 2.5. Net Primary Productivity

#### 2.5.1. Carbon 14 Rates

[35] Samples for $^{14}$C-uptake incubations measurements were collected from various depths above the 0.1% light level to assess rates of $CO_2$ incorporation in 24 h incubation experiments, following the method of *Smith et al.* [2000]. Only particulate organic carbon production was measured, and the exudation of dissolved organic matter from phytoplankton was ignored. We refer to primary productivity estimates derived from these experiments as $^{14}$C-PP. Given the length of these incubation experiments, it is likely that a significant fraction of the $^{14}$C label is recycled through autotrophic respiration, and the measurements thus reflect something closer to NPP, rather than gross primary productivity.

#### 2.5.2. SeaWiFS Primary Productivity

[36] Primary productivity was calculated from satellite using the algorithm described in detail by *Arrigo et al.* [2008b]. The algorithm computes the rate of NPP (mmol C $m^{-3}h^{-1}$) as a function of diurnal changes in spectral downwelling irradiance, sea surface temperature (°C), and chlorophyll *a* concentration (mg $m^{-3}$). SeaWiFS chlorophyll *a* is assumed to be uniform within the upper ML and decrease exponentially at greater depths [*Arrigo et al.*, 2000]. Since cloud cover inhibits chlorophyll *a* retrievals on daily timescales, 8-day images are used. The algorithm uses climatological MLDs,

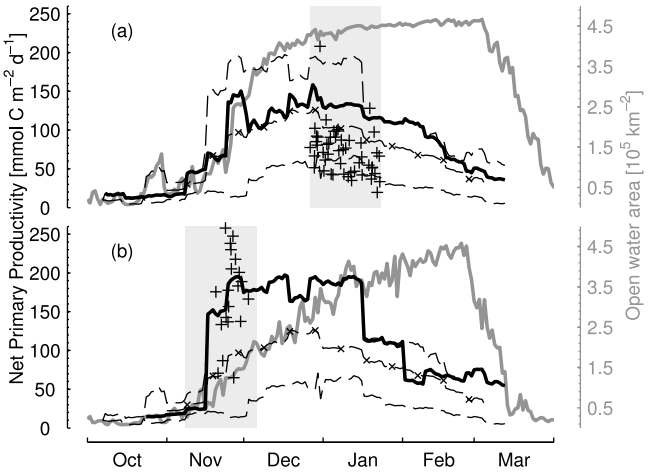


**Figure 2.** SeaWiFS-derived net primary productivity (NPP) [*Arrigo et al.*, 2008b] (black line) and PSSM-derived [*Markus and Burns*, 1995] open water area (gray line) within the region 160°E–162°W, 78°S–73.5°S for (a) 2005–2006 season and (b) 2006–2007 season. In addition to the CORSACS cruise years, the minimum, maximum (dashed) and climatological mean (crosses) NPP over the SeaWiFS record (1996–2006) are also shown. Shaded regions show the periods of time during which (a) NBP06-01 (C1) and (b) NBP06-08 (C2) were in the region. Primary productivity determined using $^{14}$C incubations are shown as pluses. One point from C2 plots off the axes: Station 61, 28 November 2006, PP = 358 mmol m$^{-2}$ d$^{-1}$.

determined using the model of *Markus* [1999]. NPP at each SeaWiFS pixel location is integrated over depth (0–100 m at 1 m intervals) and time (hourly for 24 h) to determine daily NPP (mmol C m$^{-2}$ d$^{-1}$). Phytoplankton are assumed to have a constant carbon to chlorophyll *a* ratio (88.5 g:g) [*Arrigo et al.*, 1998a]. The maximum phytoplankton net growth rate at 0°C (0.59 d$^{-1}$) is scaled to reflect temperature-dependence (first-order rate constant = 0.0633°C$^{-1}$) [*Eppley*, 1972]. SST is taken from ROISST [*Reynolds et al.*, 2002] and assumed to be constant with depth. Photoacclimation is represented using the parameterization of *Arrigo and Sullivan* [1994].

## 3. Results and Discussion

### 3.1. Large-Scale Patterns

[37] Spatially averaged SeaWiFS-derived NPP was greatest in late December in 2005 and in mid-December in 2006 (145 and 195 mmol m$^{-2}$ d$^{-1}$, respectively; Figure 2). SeaWiFS recorded the 2005–2006 primary productivity peak near the beginning of C1, when open water area was near maximal and temporal changes in areally-integrated NPP and open water area were generally low (Figure 2a). While the cruise occurred after the peak in primary productivity, the subsequent decline was slow; thus, positive rates of production were sustained through February into March. Based on these data, about 30% of the 2005–2006 seasonal total NCP had occurred when the ship arrived in the region and about 60% by the end of the cruise. Thus, time-integrated NPP occurring during the cruise was nearly equal to the total NPP prior to the cruise.

[38] During C2, the Ross Sea region was largely ice-covered, with the exception of the region near the Ross Ice Shelf (Figure 1b). Areal mean SeaWiFS-PP shows low rates of productivity during the initial portion of our survey, followed by a dramatic increase, from less than about 25 mmol m$^{-2}$ d$^{-1}$ prior to 17 November to greater than 190 mmol m$^{-2}$ d$^{-1}$, by the end of the cruise (Figure 2b). The beginning of this rise in SeaWiFS-PP is coincident with a sustained (albeit gradual) rise in open water area that continued through February (Figure 2b). Unfortunately, we do not have $^{14}$C-PP measurements prior to 20 November and thus do not resolve this dramatic change in NPP estimated from the satellite data. Additionally, the true rate of increase may not be accurately resolved by the satellite, since early-season chlorophyll retrievals were limited by clouds and sea ice. Based on the seasonal evolution of NPP captured by the satellite data, only a small percentage (0–5%) of cumulative seasonal NCP during 2006–2007 occurred prior to the C2 survey.

[39] Seasonal and annual integrals of SeaWiFS-PP suggest that the two CORSACS years had substantially different productivity regimes (Figures 3a–3d). During the 2005–2006 season (C1), NPP was concentrated in the center of the polynya region, between about 175° and 180°E and south of 76°30′S. Most of the continental shelf region was ice free by 15 December 2005, with more than 1.5 times the open water area as the same date the following year (Figure 2). As a result, the 2005–2006 bloom covered an expansive area, including a large bloom in a region not previously observed in the SeaWiFS record, north of the 1000 m isobath, centered at about 190°E (Figures 3a and 3c). SSM/I sea-ice concentration data indicate that this region, which was ice-free in 2005–2006, is typically covered.

[40] During 2006–2007 (C2 season), the ice-free area over the continental shelf was narrower in zonal extent than during the previous year. The bloom developed with two regions of intense production south of 76°S, the most significant centered on about 180°E, and another semi-distinct region to the west, at about 170°E (Figure 3b and 3d). The 2006–2007 bloom (C2) had the highest spatially-averaged rate of primary productivity from mid-November through January in the entire SeaWiFS record (Figure 2b). SeaWiFS-PP during December 2006 through mid-January 2007 was 25–30% higher than during the same period of the previous season. The physicochemical mechanisms forcing the differing bloom dynamics later in the season are not entirely clear. SSM/I ice data show that the polynya opened more gradually than usual during 2006–2007, possibly affecting stratification or contributing iron to the water column [*Sedwick et al.*, 2011]. Despite the relatively smaller bloom extent during 2006–2007, total shelf-wide production (26 Tg C) was comparable to 2005–2006 (31 Tg C).

### 3.2. Comparison of NPP Estimates

[41] During C1, the regional average satellite-derived NPP was substantially higher than mean $^{14}$C-PP (Figure 2a). When interpolated to individual cast locations, the satellite algorithm tended to overestimate primary productivity relative to $^{14}$C-PP during C1 by 67 ± 18 mmol C m$^{-2}$ d$^{-1}$ ($p < 0.001$; t-test; $n = 34$), about 90% of the C1 mean $^{14}$C-PP. The largest satellite overestimates (>100 mmol m$^{-2}$ d$^{-1}$) occurred along the western margin of the study region, proximal to sea ice (Figure 1a) and where stratification was most extreme.

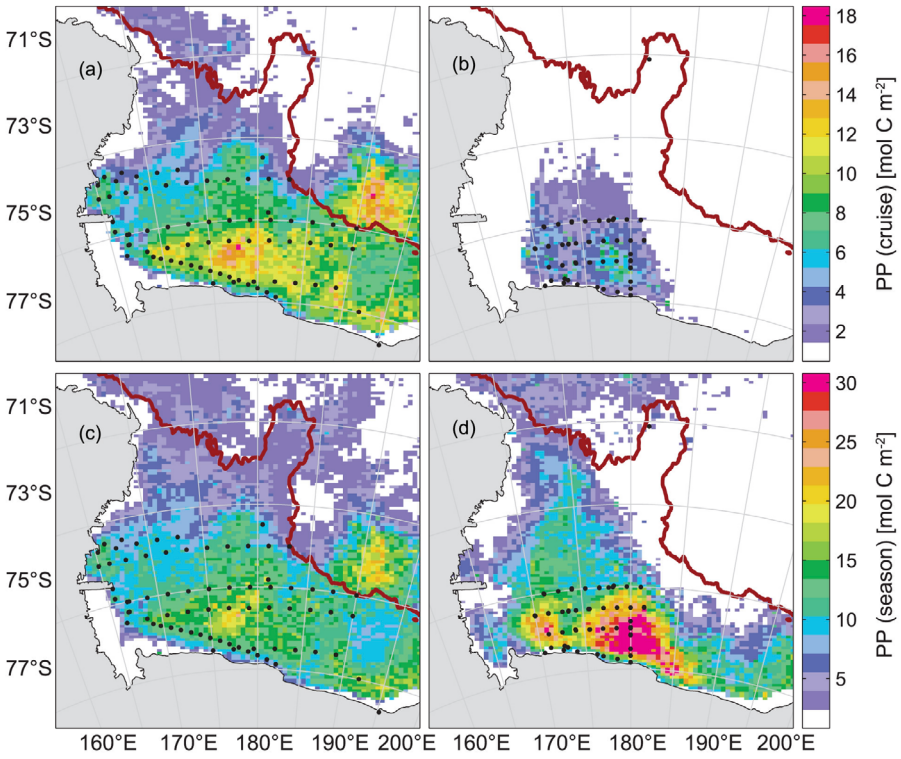


**Figure 3.** Net primary productivity integrated from (a) 1 November 2005 through 25 January 2006; (b) 1 November through 6 December 2006; (c) 1 November 2005 through 1 April 2006; and (d) 1 November 2006 through 1 April 2007. Figures 3a and 3c correspond to C1 while Figures 3b and 3d correspond to C2. White areas are regions that were ice covered or entirely obscured by clouds during the integration period.

[42] During C2, there was a reasonably good correspondence between $^{14}$C-PP and SeaWiFS-derived regional-mean NPP (Figure 2b); however, interpolating to individual cast locations reveals a bias of the same tendency as during summer, with a mean discrepancy of $60 \pm 47$ mmol C m$^{-2}$ d$^{-1}$ ($p = 0.006$; t-test; $n = 14$), about 36% of the C2 mean $^{14}$C-PP.

[43] A significant fraction of the NPP discrepancy between the satellite algorithm and $^{14}$C-PP data likely resulted from offsets between the satellite-derived and in situ chlorophyll *a* values. Mean chlorophyll *a* above 10 m depth was 1.7 mg m$^{-3}$ at casts collected during C1 and 2.4 mg m$^{-3}$ at casts collected during C2. The 8-day mean SeaWiFS chlorophyll *a* used by the algorithm were only weakly correlated with in situ HPLC chlorophyll measurements, averaged over the upper 10 m, during C1 ($R = 0.376$, $p = 0.010$) and not significantly correlated during C2. During C1, the SeaWiFS chlorophyll data exhibited a positive bias relative to the in situ measurements, tending to over-estimate surface chlorophyll by $1.15 \pm 0.6$ mg m$^{-3}$ ($p < 0.001$; t-test; $n = 46$). It should be noted that perfect agreement is not expected between satellite and in situ values, since the satellite data aggregate spatially and temporally patchy fields, and station data exhibit additional variance simply due to resolution. Nonetheless, the discrepancy in surface chlorophyll is a major source of bias in the satellite primary productivity algorithm.

[44] The assumptions regarding the vertical distribution of chlorophyll are an additional source of error in the algorithm. Figure 4a shows the relationship between surface chlorophyll and the depth integral of chlorophyll above 100 m for in situ data and the satellite algorithm. Gray shading and dashed lines on Figure 4a show the 5 to 95% quantile envelope of the $\int$ Chla *dz*-SeaWiFS Chl relationship from the *Arrigo et al.* [2008b] satellite algorithm; the range is generated by spatial and temporal variability in the climatological MLD used by the algorithm. While many of the in situ points fall within the regional envelope of the satellite algorithm, a number have chlorophyll depth integrals significantly higher than would be predicted by the satellite algorithm, likely due to deep chlorophyll maxima. Figure 4b demonstrates that much of the discrepancy between in situ $^{14}$C-PP measurements and the satellite estimates is related to error in the vertical integral of chlorophyll. This error, in turn, appears to be related to light attenuation and stratification properties of the surface ocean. Indeed, the discrepancy between the satellite and $^{14}$C productivity estimates was moderately anti-correlated with the euphotic zone depth ($R = -0.539$, $p < 0.001$) and positively correlated with the strength of upper water column stratification (mean $N^2$ above 100 m; $R = 0.540$, $p < 0.001$). The correlation of the satellite bias with stratification metrics suggest that in regions of intense stratification, the climatological water column assumptions implicit in the satellite algorithm, both the MLD and the chlorophyll distribution dependent on MLD, cause overestimation of depth-integrated chlorophyll, and hence productivity, at depth.

[45] The translation from chlorophyll biomass to productivity in carbon units is another component introducing uncertainty in the satellite algorithm. Upper water column (above 15 m) assimilation numbers (unit productivity per unit chlorophyll) computed from $^{14}$C-PP and measured in situ chlorophyll *a* were relatively constant across the study region

$(1.1 \pm 0.1$mg C (mg chl)$^{-1}$ h$^{-1}$ during C1 and $0.9 \pm 0.2$ mg C (mg chl)$^{-1}$ h$^{-1}$ during C2) and not significantly correlated with the satellite-$^{14}$C-PP difference. While we do not have a direct measure of phytoplankton carbon, Figure 4c shows the relationship between POC and chlorophyll derived from measurements for both cruises. POC measurements incorporate heterotrophic and detrital carbon pools in addition living phytoplankton. This effect is clearly evident as carbon excess in data from C1 (Figure 4c). Additionally, seasonal and regional iron limitation may affect C:Chl ratios [*Falkowski and Raven*, 2007]. The carbon to chlorophyll relationship is much tighter during C2, consistent with weak trophic coupling and detrital POC accumulation later in the season. For both C1 and C2, the slope of the POC/Chl relationship was roughly half of the C:Chl used by the satellite algorithm. Primary productivity rates predicted by the satellite algorithm are linearly dependent on the C:Chl ratio, thus it is likely that an overestimate of this ratio also contributes to the positive satellite bias.

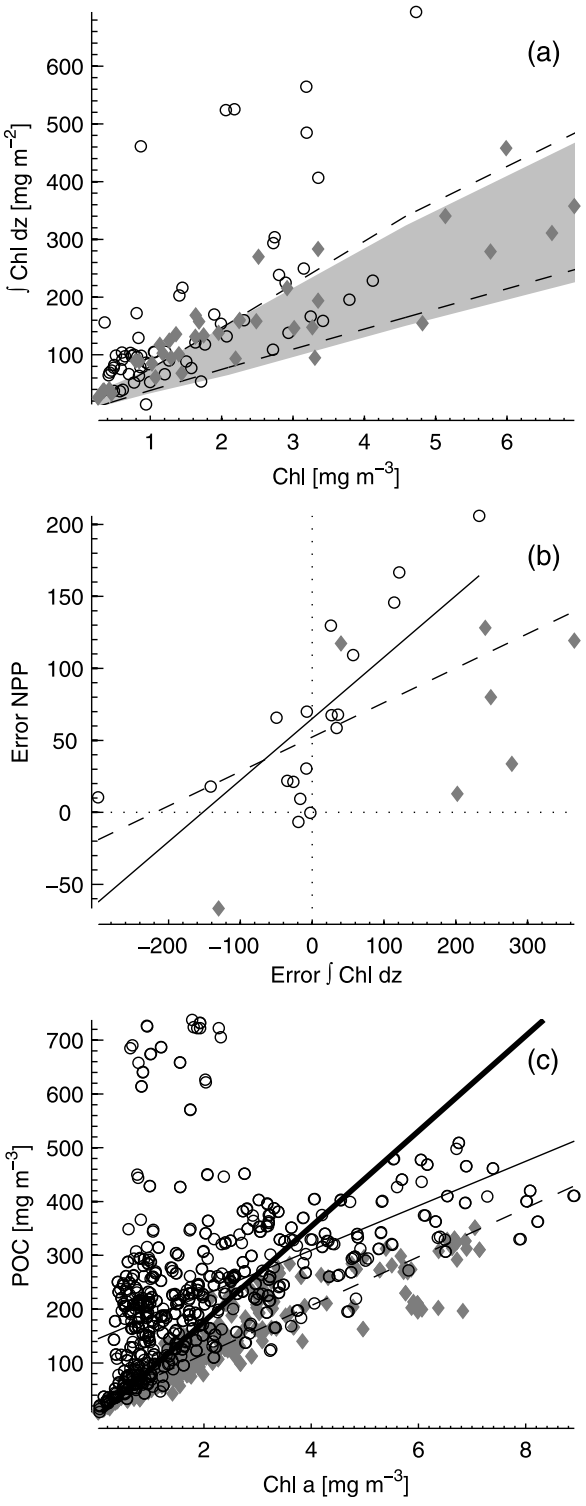


### 3.3. Water Column Structure

[46] C2, our spring cruise, included four (predominately) zonal transects; $\delta O_2$, isopycnals, and surface $pCO_2$, from these are presented in Figures 5a–5d. Figures 6a–6e show similar transect data collected during C1, the summer cruise. We have chosen to present CTD-derived $O_2$ data in Figures 5 and 6 because the vertical sampling resolution is much greater than for *s*DIC or TIN collected from rosette bottles. For both cruises, oxygen variability was tightly coupled to *s*DIC ($R = -0.906$, $p < 0.001$; see Figure 7) and TIN ($R = -0.891$, $p < 0.001$). Additionally, we present only surface $pCO_2$ data, due to gaps in the $\Delta O_2$/Ar data and the tight coupling of $pCO_2$ and $\Delta O_2$/Ar. A regression of surface $pCO_2$versus $\Delta O_2$/Ar yields a slope of $-7.47 \pm 0.05$ ($r^2 = 0.774$) for C1 and a slope of $-6.15 \pm 0.02$ ($r^2 = 0.966$) for C2. Tables S1 and S2 in the auxiliary material summarize the data from stations along these transects.[1]

[47] Later season deficit integrals provide more robust NCP estimates than early season integrals, primarily because the uncertainty in initial conditions is a less significant fraction of the total drawdown. For instance, a minimum estimate of pre-bloom surface water *s*DIC variability is the standard

[1]Auxiliary materials are available in the HTML. doi:10.1029/2009JC005954.

**Figure 4.** (a) Depth-integrated chlorophyll versus surface chlorophyll *a*. Points show in situ data from the two CORSACS cruises, where we use the mean chlorophyll *a* above 10 m to represent surface chlorophyll. Gray shading and dashed lines show the 5 to 95% quantile envelope of the ∫Chla *dz*-SeaWiFS Chl relationship from the *Arrigo et al.* [2008b] satellite algorithm for the Ross Sea region (160°E–162°W, 78°S–73.5°S) during C1 (gray shading) and C2 (dashed lines). (b) SeaWiFS-PP minus $^{14}$C-PP versus the difference between the vertical integral of chlorophyll *a* used by the satellite algorithm and the in situ observations. The solid black line ($y = (65 \pm 21) - (0.43 \pm 0.20)x$, $r^2 = 0.565$) summarizes the discrepancy relationship during C1; this relationship was not significant during C2. The dashed line ($y = (52 \pm 24) - (0.24 \pm 0.15)x$), $r^2 = 0.312$ shows the overall relationship for both cruises. (c) Particulate organic carbon versus chlorophyll *a* during C1 and C2. The thin solid line shows the least squares relationship for C1 data ($y = (144 \pm 13) + (41 \pm 4.8)x$, $r^2 = 0.256$) whereas the dashed line shows the relationship for C2 ($y = (25 \pm 3.4) + (45 \pm 1.4)x$, $r^2 = 0.838$). The thick solid line shows the ratio used by the *Arrigo et al.* [2008b] satellite algorithm (88.5). In each plot, circles show data from C1, while diamonds show data from C2.

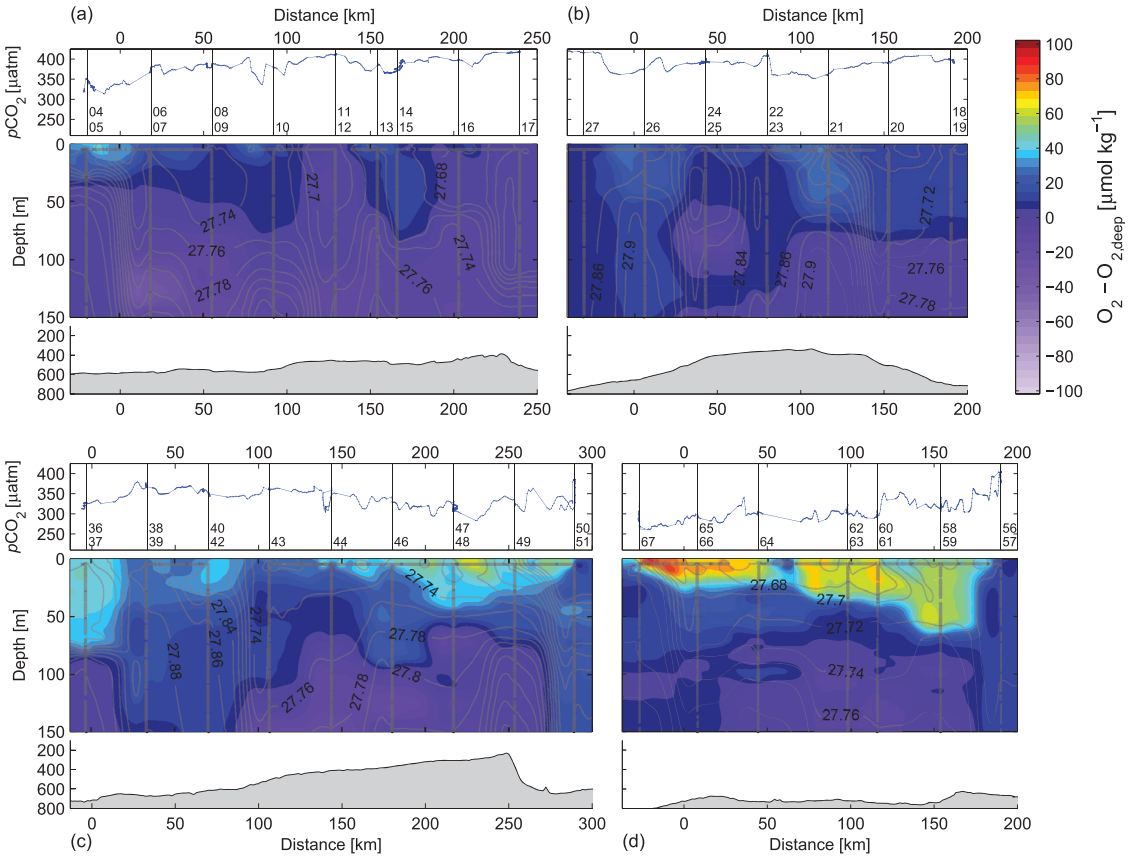


**Figure 5.** Spring (C2) transects. (a) 76°S, occupied 15–18 November 2006; (b) 77°S, occupied 18–20 November 2006; (c) 76°30′S occupied 23–26 November 2006; and (d) along the Ross Ice Shelf, occupied 27–29 November 2006. Color shows $\delta O_2$ concentration and contours show density structure presented as $\sigma_\theta$. $\delta O_2$ is defined as $[O_2]$ minus mean $[O_2]$ below 200 m for the whole cruise (Table 2). Gray dots show the location of data points used for griding. Points along the surface between stations are from underway temperature, salinity, and $\Delta O_2/Ar$ data. $[O_2]$ at these locations is predicted from a regression of mean $[O_2]$ above 10 m on $\Delta O_2/Ar$ at station locations. This yields a robust relationship: $\langle O_2 \rangle_{10m} = (338.98 \pm 2.90) + (3.187 \pm 0.26)\ (\Delta O_2/Ar)$, $r^2 = 0.900$ for C2 and $\langle O_2 \rangle_{10m} = (349.96 \pm 4.28) + (3.355 \pm 0.36)\ (\Delta O_2/Ar)$, $r^2 = 0.784$ for C1 (excluding three outlier stations: 79, 89 and 97). Data are gridded using a Laplace gradient-minimizing technique. Surface $pCO_2$ is plotted in each top panel; bathymetry along the section from *Amante and Eakins* [2008] is plotted in each bottom panel. The $x$-axis is the distance along the transect from the easternmost point on the section. All sections are plotted with north into the page, although in some cases the section was occupied from east to west.

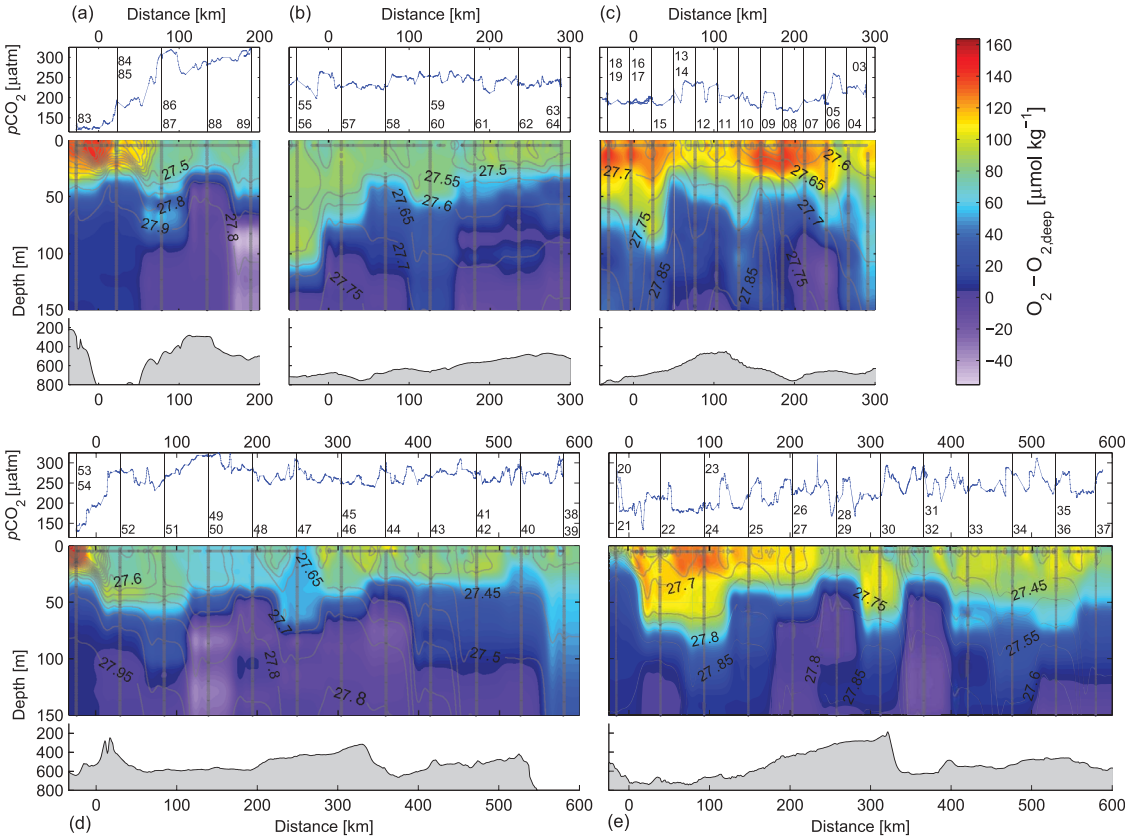


**Figure 6.** Summer (C1) transects. (a) 74°42′S, occupied 19–20 January 2006; (b) 77°30′S, occupied 10–12 January 2006; (c) along Ross Ice Shelf, occupied 28–30 December 2005; (d) 76°00′S, occupied 5–9 January 2006; and (e) 76° 30′S, occupied 31 December 2005 to 5 January 2006. Color shows $\delta O_2$ concentration and contours show density structure. Contour interval is 0.05 for all plots except Figure 4a, which has a contour interval of 0.1. Surface $tpCO_2$ is plotted in each top panel; bathymetry from *Amante and Eakins* [2008] is plotted in each bottom panel. See Figure 5 caption for further details.

deviation of *s*DIC below 200 m, 4–5 $\mu$mol kg$^{-1}$(Table 2). This variability corresponds to about ± 0.5mol C m$^{-2}$, assuming a uniform vertical distribution, integrated above 100 m: about 15% of the mean C1 *s*DIC drawdown and 40% of C2 drawdown. Thus, while the consistency of *s*DIC and nutrient concentrations below 200 m between cruises (Table 2) supports the use of deep water as a proxy for winter water conditions, variability in these properties is a significant source of uncertainty when drawdown is low. Gas exchange represents another, albeit minor, source of uncertainty in NCP estimates. Using data from both cruises, we find that gas exchange scaled linearly with NCP, with flux into the ocean increasing by 50 ± 10 mmol m$^{-2}$ per mol C m$^{-2}$ increase in NCP above 100 m (Figure 8). In other words, $F_{co_2}$ comprised about 5 ± 1% of NCP.

### 3.3.1. Early Season Tracer Distributions

[48] The first two transects during C2 (76°S and 77°S; Figures 5a and 5b) occurred largely prior to the dramatic rise in primary productivity evident in the SeaWiFS data. Stations within these two sections display SSM/I ice cover between about 20% and 70%, surface $pCO_2$ (with a few exceptions) at or above atmospheric equilibrium, and $\Delta O_2$/Ar well below saturation (Table S1). Correspondingly, much of the upper water column along these sections had low or negative $\delta O_2$concentrations, although integration of both *s*DIC and $O_2$ showed that water above 100 m had net positive production at all casts except at station 11/12.

[49] Data collected along 76°30′S (23–26 November; Figure 5c) illustrate the rapid progression from winter conditions to open water bloom conditions. While mean ice coverage along this section remained as high as 40%, positive $\delta O_2$, increased surface $\Delta O_2$/Ar and $pCO_2$ consistently below atmospheric saturation show a clear signal of net productivity (Table S1). This productivity was also evident in increased $O_2$ concentration in the water column, with depth-integrated values exceeding 2 mol C m$^{-2}$ in several locations. The most significant $O_2$ accumulation is evident approaching both ends of this transect.

[50] The final transect of C2 (along the Ross Ice Shelf; Figure 5d) had the highest mean $\delta s$DIC, $^{14}$C-PP, as well as the first surface $pCO_2$ measurements below 300 $\mu$atm and first positive $\Delta O_2$/Ar values (Table S1). Additionally, we observed the largest deficit integrals in this region. These large deficit integrals may in part be due to earlier bloom inception (and later sampling); at the time of sampling, stations along this section had experienced 10 or more additional ice-free days than any prior station on the cruise. The region along the Ross Ice Shelf was ice free for the entire cruise duration (Figure 1b); in fact due to high winds near the continent, this region is often ice-free during winter.

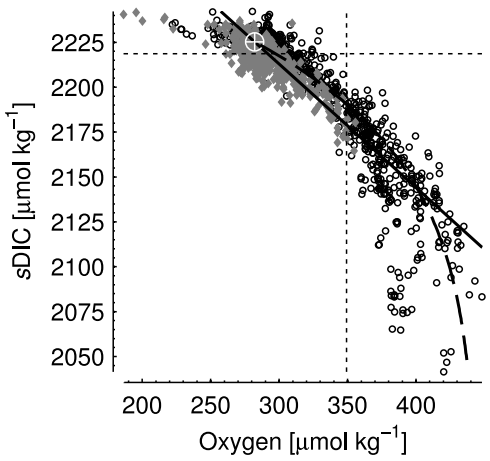


**Figure 7.** *s*DIC concentrations plotted versus dissolved oxygen for C1 (circles) and C2 (diamonds). Circled cross illustrates the mean properties for both cruises below 200 m (Table 2), the presumed starting condition of the early spring water column. The solid black line illustrates the evolution of DIC and oxygen under the influence of biology alone, assuming − $O_2$:C = 170:117. The dashed line shows a box model solution for a 50 m mixed layer, forced by constant wind (5 m $s^{-1}$) and NCP (85 mmol $m^{-2}$ $d^{-1}$). The vertical and horizontal dotted lines show the approximate saturation concentration for oxygen and DIC, respectively, with salinity = 34.5, temperature = 0°C, and alkalinity = 2347 $\mu$mol $kg^{-1}$.

[51] In casts collected during C2, $\delta s$DIC-NCP above 100 m varied between about 0.1 and 2.5 mol C $m^{-2}$ (mean 1.2 ± 0.6 mol C $m^{-2}$). Satellite NPP and the initial C2 casts indicate the NPP prior to the cruise was minimal; thus water column integrals should mostly reflect NPP occurring during the cruise. Indeed, we see a relatively tight coupling between active biological processes and in situ tracer distributions. $^{14}$C-PP and $\delta s$DIC-NCP above 100 m are positively correlated during C2 ($R$ = 0.618, $p$ = 0.005). Similarly, depth-integrated chlorophyll *a* is strongly correlated to NCP during

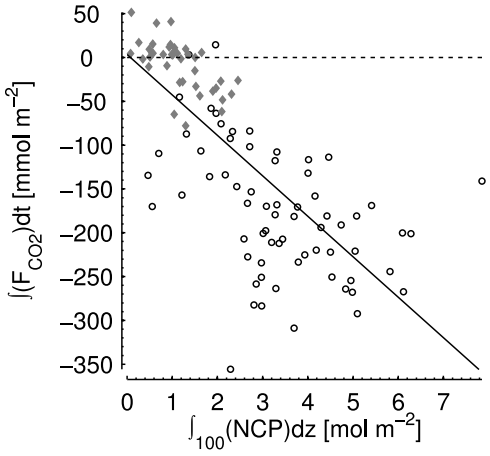


**Figure 8.** Time-integrated air sea exchange plotted against depth-integrated NCP above 100 m for C1 (circles) and C2 (diamonds). The solid line summarizes the overall relationship ($y$ = − (1.3 ± 26) + (46 ± 9)$x$, $r^2$ = 0.500, $p$ < 0.001).

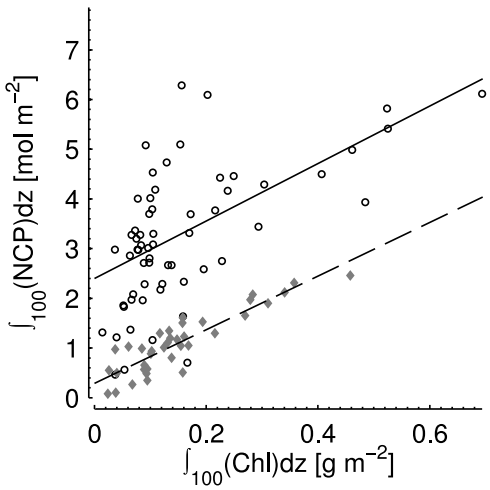


**Figure 9.** Net community production versus depth integrated chlorophyll for C1 (circles, solid line) and C2 (diamonds, dashed line). For C1, the relationship is summarized by $y$ = (110 ± 41) + (21 ± 12)$x$, $r^2$ = 0.165, $p$ < 0.001; similarly for C2, $y$ = + (25 ± 16) + (29 ± 13)$x$, $r^2$ = 0.370, $p$ < 0.001.

C2 ($R$ = 0.892, $p$ < 0.001; Figure 9), confirming that active productivity is a primary factor structuring early season variance in *s*DIC, $O_2$, and nutrient distributions.

[52] The distribution of primary productivity reflected in Figures 5a–5d can be attributed to differences in stratification across our sampling region. In general, spring MLDs were relatively deep, although we did encounter several localized regions with shallow (i.e., <50 m) mixed layers (Table 1). The subsurface density structure shows strong frontal features near station 4/5 (Figure 5a), station 21 (Figure 5b), and stations 40/42 and 49 (Figure 5c). There is enhanced stratification west of these fronts, which is accompanied by $O_2$ accumulation in the upper water column, resulting in a pattern qualitatively similar to the SeaWiFS-PP distribution (Figure 3), with higher productivity occurring near the ends of transects approaching the ice edge interior to the polynya. Ekman advection was likely responsible for enhanced stratification, and therefore enhanced productivity due to higher mean irradiance, adjacent to upper the fronts (M. C. Long et al., Control of the early season bloom inception in the Ross Sea, Antarctica by Ekman restratification, submitted to *Global Biogeochemical Cycles*, 2011).

#### 3.3.2. Summer Tracer Distributions

[53] Hydrographic conditions were distinctly different in the summer time survey (C1), due to dramatically lower sea ice coverage and increased upper ocean stratification. Mean MLDs were shallower during the summer cruise and the difference between spring and summer MLDs increased with greater values of the $\Delta\sigma_t$ criterion, indicating enhanced upper ocean stratification (Table 1) and ML stability: the mean value of $N^2$ at the MLD was approximately sixfold greater during C1 relative to C2 (Table 1). In contrast to the spring, ice melt played a primary role controlling mixing depths and the broad spatial patterns of NCP and nutrient drawdown during C1.

[54] Large local excursions in surface salinity along the western margin of the study region are correlated with

**Table 1.** Various Mixed Layer Depths, Density ($\sigma_t$) and Buoyancy Frequency ($N^2$) at the Base of Mixed Layer and Percent of $\delta s$DIC Found Above the Mixed Layer Depth

| | MLD (m) | | $\sigma$ at MLD (kg m$^{-3}$) | | $N^2$ at MLD ($10^{-4}$s$^{-2}$) | | $\delta s$DIC Above MLD[a] (%) | |
|---|---|---|---|---|---|---|---|---|
| Criterion | Spring | Summer | Spring | Summer | Spring | Summer | Spring | Summer |
| $\Delta\sigma$ = 0.02 | 62 ± 51 | 24 ± 16 | 27.74 ± 0.1 | 27.50 ± 0.2 | 0.37 ± 0.42 | 1.6 ± 3.5 | 71.7 ± 32.1 | 58.8 ± 37.5 |
| $\Delta\sigma$ = 0.03 | 71 ± 53 | 26 ± 18 | 27.75 ± 0.1 | 27.51 ± 0.2 | 0.38 ± 0.51 | 1.6 ± 3.5 | 78.0 ± 29.7 | 62.4 ± 36.5 |
| $\Delta\sigma$ = 0.05 | 99 ± 65 | 33 ± 23 | 27.76 ± 0.1 | 27.53 ± 0.2 | 0.3 ± 0.52 | 1.7 ± 3.6 | 86.0 ± 30.9 | 70.0 ± 34.4 |
| $\Delta\sigma$ = 0.07 | 132 ± 83 | 39 ± 30 | 27.78 ± 0.1 | 27.55 ± 0.2 | 0.24 ± 0.47 | 1.7 ± 3.7 | 92.2 ± 31.9 | 76.6 ± 33.6 |
| $\Delta\sigma$ = 0.1 | 178 ± 114 | 52 ± 40 | 27.80 ± 0.1 | 27.58 ± 0.2 | 0.21 ± 0.35 | 1.6 ± 3.8 | 92.6 ± 40.8 | 84.7 ± 33.8 |
| $\Delta\sigma$ = 0.125 | 208 ± 126 | 63 ± 47 | 27.82 ± 0.1 | 27.60 ± 0.2 | 0.22 ± 0.38 | 1.6 ± 3.8 | 82.6 ± 44.9 | 88.8 ± 33.0 |

[a]Deficit integral above the MLD relative to the deficit integral above 100 m.

shallow mixed layers, intense $O_2$ accumulation and *s*DIC drawdown. This is shown best along the 74°42′S transect (Figure 6a), which extends into Terra Nova Bay, north of the Drygalski Ice Tongue. Surface water at stations 83 and 84/85 have low surface salinity and hence low density, likely due to sea ice and possible glacial melt contributions. A shallow lens of freshwater is also evident at station 20/21 (Figure 6e) and station 53/54 (Figure 6d), which are at the far western end of 76°30′S and 76°S, respectively. Stratification is extreme at all these stations, with MLDs defined on the basis of $\Delta\sigma_t$ = 0.125 not exceeding 13 m. High surface $O_2$ was observed at all the highly stratified cast locations (Figures 6a, 6d, and 6e).

[55] Intense surface drawdown in shallow settings (e.g., station 83: $pCO_2$ = 129 $\mu$atm, $\Delta O_2$/Ar > 23%) likely reflects a favorable light regime and the potential for ice-melt derived iron enrichment [*Sedwick et al.*, 2011]. Conversely, less intense surface drawdown in deeply mixed settings may be a consequence of light limitation. Drawdown concentration is dependent on MLD; for instance, during C1, ML *s*DIC deficit concentration (i.e., mol kg$^{-1}$) decreased about 0.9 ± 0.4 $\mu$mol kg$^{-1}$ for every meter increase in MLD (Figure 10a). The slope of this relationship is larger than that observed during C2 (0.1 ± 0.04 $\mu$mol kg$^{-1}$ m$^{-1}$), reflecting the fact that deficit concentrations from C2 represent a much smaller fraction of the season.

[56] While clear spatial patterns were observed in volumetric surface drawdown (i.e., mol kg$^{-1}$ deficits), surface drawdown intensity is not necessarily indicative of greater water column deficit integrals (Figure 10b). The shallow mixed layers in the west had intense surface drawdown: very low surface $pCO_2$ and elevated $\Delta O_2$/Ar; however, the greatest column integrated $\delta s$DIC values above 100 m (Table S2) were found in more deeply mixed settings. For instance, station 55/56 along 77°30′S (Figure 6b) had the greatest $\delta s$DIC during C1, with relatively mild drawdown intensity distributed over the full upper 100 m.

[57] Overall, data from C1 show a mean increase in depth-integrated $\delta s$DIC as a function of MLD ($\Delta\sigma_t$ = 0.05) of 0.04 ± 0.01 mol C m$^{-2}$m$^{-1}$ ($r^2$ = 0.483) (Figure 10b). Theoretically, depth integrated drawdown should increase with increasing MLD, reach a maximum, and then begin to decline due to light limitation. While data from C2 are not inconsistent with this paradigm, data from C1 do not show significant evidence of a decline in drawdown with increasing MLD, perhaps because we did not sample mixed layers deep enough to incur light limitation (Figure 10b). An additional possibility relates to the magnitude of respiration. If respiration is weak relative to the rate of NPP, the mechanism causing a reduction in depth-integrated drawdown with increasing MLD is limited; in fact, deficit concentrations might be mixed to depth and persist, leading to apparent increases in depth integrals with increasing mixing depth. Prior work in the Ross Sea has shown bacterial respiration to be low, relative to rates of NPP [*Craig et al.*, 1999; *Azzaro et al.*, 2006], thus this explanation seems plausible. It is not clear how to reconcile this finding, however, with the inference that respiration is of comparable magnitude to NCP (see below). While subsurface structure is clearly related to productivity patterns during C2, there is no

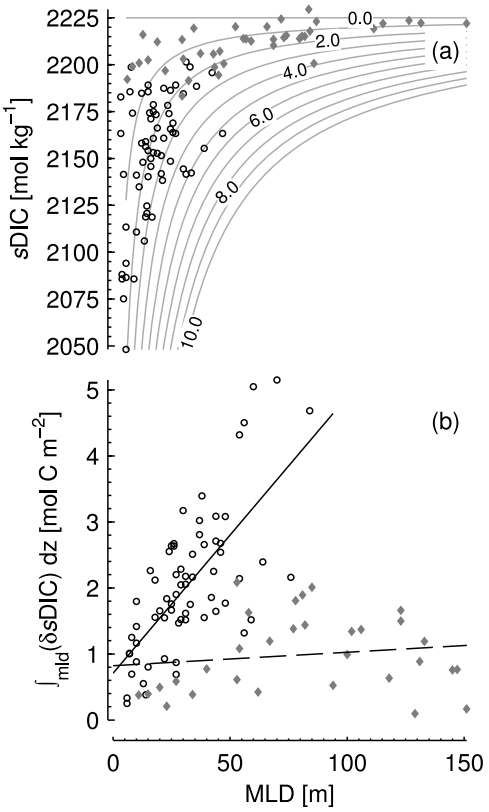


**Figure 10.** (a) Mixed layer *s*DIC as a function of mixed layer depth (MLD) for C1 (circles) and C2 (diamonds). The contours show the theoretical relationship for NCP rates between 0 and 10 mol C m$^{-2}$, presuming all NCP occurs within the mixed layer. (b) Depth-integrated *s*DIC drawdown as a function of MLD ($\Delta\sigma_t$ = 0.05) for C1 (circles) and C2 (diamonds). The black line shows the least squares relationship for C1 ($y$ = (0.71 ± 0.40) + (0.04 ± 0.01)$x$, $r^2$ = 0.484, $p$ < 0.001). The dashed line shows the same relationship for C2, the slope of which is not significantly different from zero.

significant relationship between ML depth-integrated $\delta s$DIC and MLD (Figure 10b).

[58] In situ $\delta s$DIC-based NCP (equation (3)) above 100 m ranged from 0.5 to 8 mol C $m^{-2}$(mean 3.4 ± 1.5 mol C $m^{-2}$) during C1, with no clear temporal trends. NCP during C1 was maximum along the quasi-zonal ice shelf section (Figure 6c) and along 77°30′S (Figure 6b), both just south of the SeaWiFS-PP maximum (Figures 3a and 3c). Relative to data from our spring cruise, observations collected later in the season demonstrate a decoupling between active biological processes and tracer distributions as the season progresses. For example, the correlation between NCP and depth-integrated chlorophyll *a* ($R = 0.504$, $p < 0.001$) was not as strong during C1 as during C2. Interestingly, while the strength of correlation is reduced for C1, the slope of the NCP-chlorophyll relationship is very similar between cruises (Figure 9); the intercept is greater for C1, reflecting the accumulation of a seasonal drawdown signal. $^{14}$C-PP and NCP during C1 were not significantly correlated. Both the scatter in the NCP-chlorophyll relationship and the lack of correlation with $^{14}$C-PP during summer demonstrate that much of the NCP signal present in the later season water column has accrued over time, been subjected to ocean mixing, and is therefore decoupled from instantaneous biological processes.

[59] Vertical motions may be important in structuring the later-season NCP signal. For instance, station 31/32 (Figure 6e) had nearly the lowest NCP measured during C1 while the station immediately to the west, (station 30, about 50 km away) had the second highest NCP measured on the cruise. Between these two stations is a front, apparent in the isopycnals shown on Figure 6e, resulting in a difference in surface water density of 0.23 kg $m^{-3}$ between station 30 and 31/32. The presence of such a front and the distribution of $\delta O_2$ concentrations at depth (Figure 6e) suggest that upwelling of low $O_2$, carbon-rich waters is partially responsible for the very low NCP at station 31/32. Changes in mixing depths with time likely play an important role in distributing the NCP signal.

### 3.4. Respiration

[60] Community respiration can, in principle, be determined by the difference between NCP and NPP (equation (1)). During C2, $\delta s$DIC-NCP increased by about 80 ± 30 mmol C $m^{-2}$ $d^{-1}$. This rate of change should reflect the balance of concurrent NPP and community respiration rates, although some portion of the trend may be due to spatial variability. Regardless, the mean euphotic-zone $^{14}$C-PP during the cruise was approximately 180 ± 70 mmol C $m^{-2}$ $d^{-1}$, roughly double the rate of increase in the seasonally-integrated NCP (i.e., mol $m^{-2}$) as determined by $\delta s$DIC. While the $^{14}$C-PP method can incorporate heterotrophic respiration, and therefore underestimate NPP [*Marra*, 2002], the comparison between NCP and $^{14}$C-PP suggests that NCP and losses due to community respiration are of the same order of magnitude.

[61] Satellite data provide our only estimate of NPP on the seasonal timescale reflected by C1 deficit integrals, although NCP and time-integrated (beginning 1 November) SeaWiFS-PP were not significantly correlated at individual cast locations. Physical processes (i.e., lateral advection) are likely to have redistributed the signal of seasonal NCP measured during C1, which may partially explain this poor correlation. Nevertheless, the mean NPP from satellite data interpolated to station locations and integrated from 1 November to the respective sampling date is 5.3 ± 2.0 mol C $m^{-2}$, indicating that seasonally integrated respiration on the continental shelf was of similar magnitude as mean NCP (3.4 ± 1.5 mol C $m^{-2}$), about ~2 mol C $m^{-2}$ by the end of C1.

[62] Data from both cruises indicate that NCP accounted for about half of mean primary productivity over the respective integration periods. Measurement limitations and spatial heterogeneity, reflected in the large error bars, limit confidence in this result; however, previous studies in the Ross Sea are not inconsistent with this pattern. *Bender et al.* [2000], for instance, determined a net to gross production ratio of 0.32, based on in vitro incubations. *Asper and Smith* [1999] used incubation techniques to measure the *f*-ratios at locations in the southwestern Ross Sea ranging from 0.44 to 0.89 (the *f* ratio is equivalent to the ratio of NCP to NPP at steady state [*Laws et al.*, 2000]). While the higher end of these estimates reflects little respiration loss, the lower end is consistent with respiration approximately equivalent to NCP. Respiration is an important term determining the fate of fixed carbon on the Ross Sea continental shelf. Future studies should make concerted efforts to close this gap by repeated measurements on the same evolving water mass.

### 3.5. Nutrient Removal Stoichiometry

[63] In general, we find that $\delta s$TIN and $\delta O_2$ integrals above 100 m provide NCP estimates based on C:O and C:N stoichiometry that are largely consistent with $\delta s$DIC (Figure 11). $\delta s$DIC-based NCP tends to be about 80% of $\delta s$TIN, when using the stoichiometric C:N ratio of *Dunbar et al.* [2003]. The ratio of $\delta s$DIC (corrected for gas exchange) to $\delta s$TIN above 100 m during C1 was 5.8 ± 0.6 ($r^2 = 0.835$). This ratio is sensitive to gas exchange, and underestimation of sea-air $F_{co_2}$ may cause underestimation of the true drawdown ratio. Fundamentally, the gas exchange parameterization is highly uncertain, particularly where sea ice dynamics affect the boundary layer. Additionally, the use of daily-mean wind speeds may cause an underestimation bias in the gas exchange calculation if wind speeds are highly variableon shorter timescales. Other investigators have found low wind biases and spurious atmospheric pressure trends in the NCEP/NCAR fields [e.g., *Hines et al.*, 2000; *Hertzog et al.*, 2006; *Arrigo et al.*, 2008a]. Indeed, during C1, the NCEP/NCAR daily winds were about 80 ± 40% of the ship's daily average winds and about 70 ± 30% during C2. As can be seen in Figure 12b, the C:N ratio is not constant through the water column during C1, with the upper portion above about 30 m showing an apparent excess of N. This suggests that the effect of gas exchange is most significant in the upper water column. If we multiply the computed gas-exchange by a factor of four, the C:N ratio is increased to 6.2, still significantly lower than the assumed ratio of 7.23. Thus gas exchange alone does not likely account for the discrepancy in C:N ratios.

[64] The ratio of POC to PON was 6.3 ± 0.08 ($r^2 = 0.976$) for samples collected during C1 and 6.0 ± 0.05 ($r^2 = 0.991$) for C2. Since preferential remineralization of N is likely to have caused an increase in this ratio, rather than a decrease, this further corroborates indications that the C:N stoichiometry differs from the *Dunbar et al.* [2003] value of 7.23. This

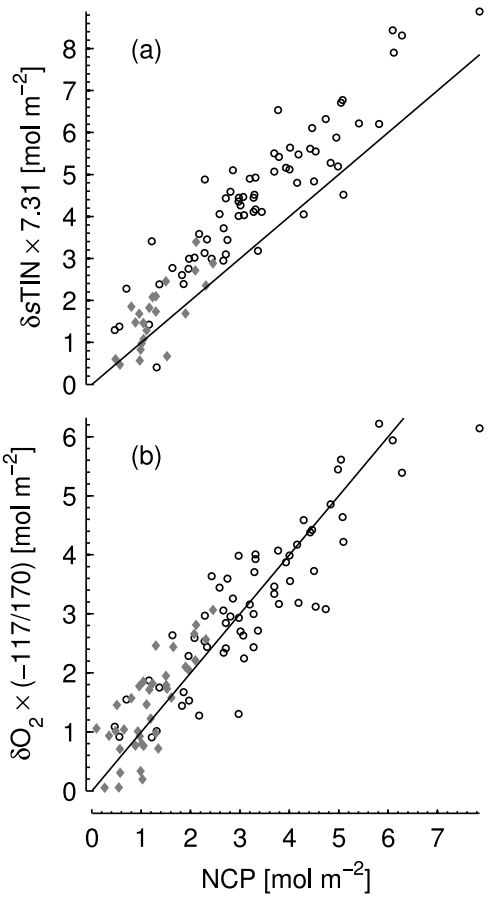


**Figure 11.** Net community production estimates from (a) total inorganic nitrogen drawdown and (b) oxygen accumulation, converted to carbon currency as described in the text and plotted versus *s*DIC drawdown above 100 m, corrected for gas exchange. Circles show data from C1; diamonds show data from C2. The lines show a 1:1 relationship.

latter ratio was determined from several cruises to the Ross Sea in the late 1990s. It is possible that our lower value is representative of interannual variability in C:N utilization in the Ross Sea, perhaps dependent on the particular assemblage composition of a given year. Understanding the mechanisms driving interannual variability in nutrient utilization will be important for accurate biogeochemical modeling.

[65] While the column integrals of $\delta O_2-$ and $\delta s$DIC-based NCP are quite consistent (Figure 11b), a careful examination of the $O_2$-*s*DIC relationship with depth (Figure 12a) shows that the slope of the $O_2$:C relationship deviates significantly from the assumed biological ratio of −170:117 in the upper water column during C1. This is also evident as a departure from linearity in the $O_2$/DIC relationship in C1 samples shown on Figure 7. Deviations from the biological ratio are due to preferential $O_2$ gas exchange in surface waters. At the beginning of the season, surface waters are undersaturated with respect to $O_2$, thus gas exchange contributes oxygen to the surface ocean. This results in an excess of oxygen relative to DIC. Later in the season (Figure 7), oxygen accumulates in surface waters to supersaturated conditions, but gas exchange acts to restore $O_2$ concentrations to atmospheric equilibrium, resulting in a deficiency of oxygen relative to DIC.

[66] The close correspondence of $O_2$ and *s*DIC deficit integrated to 100 m suggests, however, that ventilation of the entire biologically-influenced portion of the water column does not occur quickly enough to provide an imprint of preferential $O_2$ gas exchange (Figure 12a). Additionally, since the sign of the $O_2$ gas flux term reverses, early season $O_2$ influx may compensate somewhat for later season degassing and the gas flux terms thus partially cancel out over a seasonal cycle. The fact that the early season water column is undersaturated with respect to oxygen indicates that wintertime gas exchange is relatively insignificant; this is an important observation, since the efficiency of air sea exchange in ice covered regions is not well understood and the reductions in $CO_2$ efflux during winter are critical to maintaining the Ross Sea as a net annual carbon sink [*Sweeney*, 2003].

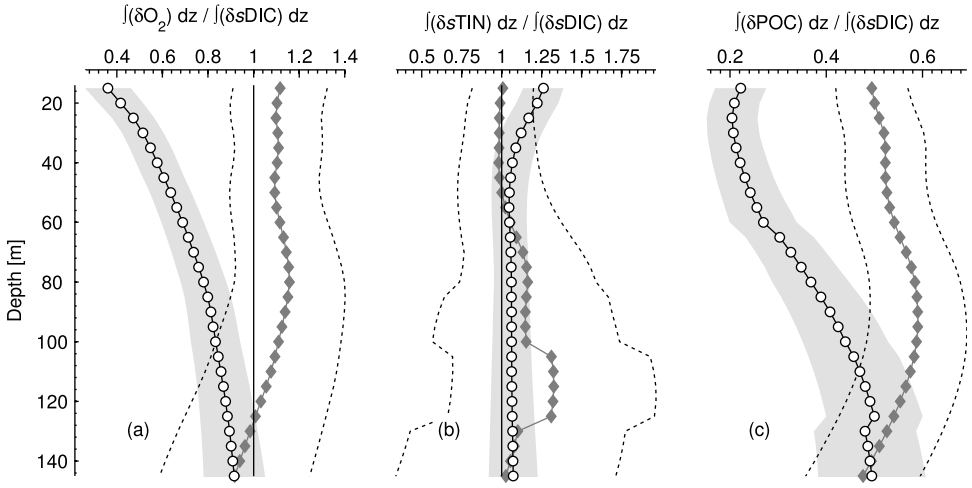


**Figure 12.** Slope of the relationship between (a) $\delta O_2 \times -117/170$, (b) $\delta s$TIN × 7.23, and (c) $\delta$POC versus $\delta s$DIC as a function of depth for C1 (circles) and C2 (solid diamonds). Shaded regions (C1) and dashed lines (C2) show the 95 % confidence limits on the slope estimates. Note that what is plotted is the slope of the relationship between the two integrals above depth *z*, which is slightly different from the ratio of these two quantities, since the intercept is not constrained to be zero.

**Table 2.** Mean Properties Plus or Minus Standard Deviation Below 200 m on the Ross Sea Continental Shelf During Summer (CORSACS-I) and Spring (CORSACS-II) Cruises[a]

| Constituent | Summer | Spring |
|---|---|---|
| $O_2$ | 289.5 ± 5.8 | 279.2 ± 4.4 |
| *s*DIC | 2225 ± 4 | 2224 ± 5 |
| *s*TIN | 30.6 ± 0.9 | 30.1 ± 0.6 |
| $sPO_4^{3-}$ | 2.2 ± 0.1 | 2.2 ± 0.1 |
| $sSi(OH)_4$ | 80.7 ± 2.7 | 80.6 ± 0.9 |
| POC | 3.0 ± 3.6 | 1.1 ± 0.6 |
| Salinity | 34.7 ± 0.1 | 34.7 ± 0.1 |
| Temperature | −1.9 ± 0.1 | −1.9 ± 0.1 |

[a]C1 averages only include date from the smaller regional footprint of C2. Units for all constituents except salinity and temperature (°C) are $\mu$ mol kg$^{-1}$. With the exception of $SiO_2$, which is about 9 $\mu$ mol kg$^{-1}$ higher, our deep measurements are similar to the early spring mean concentrations (between 100 and 400 m) reported by *Sweeney et al.* [2000].

[67] The standing stock of POC accounts for a modest fraction of $\delta s$DIC during C1 and C2 (Figure 12c). Above ~50 m, just over 20% of the carbon deficit can be accounted for by carbon in the POC pool, while 40–50% of $\delta s$DIC is present as POC above 150 m, consistent with downward transport of the season's NCP. The C2 $\delta$POC($z$)/$\delta s$DIC($z$) profile shows a generally uniform distribution of POC relative to carbon deficit with depth. About 60% of the $\delta s$DIC above 150 m is present as POC. POC declines substantially below 200 m (Table 2). These numbers are somewhat lower than those reported by others; for instance, *Arrigo et al.* [2000] reported finding 70–100% of $\delta s$DIC accounted for by particulate matter during a mid-December through early January cruise. *Sweeney et al.* [2000] found 65% of NCP present as POC in the upper water column (above 100 m) in mid-February. These observations suggest that NCP is likely an overestimate of export flux, since a sizable fraction of NCP tends to remain as POC, vulnerable to recycling in the upper water column. Dissolved organic carbon production in the Ross Sea is thought to be modest and play a small role in export production [*Carlson et al.*, 2000]. Peak particle fluxes in the Ross Sea have been measured via sediment traps to occur in autumn [*Dunbar et al.*, 1998; *Smith and Dunbar*, 1998; *Collier et al.*, 2000; *Langone et al.*, 2003], well after typical bloom senescence. Quantitative studies tracking the fate of seasonal NCP are lacking in the Ross Sea.

### 3.6. Temporal Evolution of Biogeochemical Signals

[68] Presuming the assumptions are met, the WPV method returns a weighted average of NCP rates over the time period used in the gas exchange calculation. Regarding the assumption of steady state, the initial undersaturation of $O_2$ in the early season water column has important implications for the calculation of ML NCP using the WPV method. The method assumes that the ML is at steady state with respect to $O_2$ in the surface ocean. In the undersaturated conditions present during the C2 survey, both NCP and air-sea exchange contribute to increasing ML $O_2$ concentrations and the assumption of steady state implicit in equation (7) is not applicable. As $O_2$ accumulates in the surface ocean, concentrations begin to approach steady state, where $O_2$ concentrations are large enough for efflux to balance NCP (Figure 13). The time required to reach steady state from undersaturated initial conditions can be found using an analytical expression for ML $O_2$ by integrating equation (6). Under steady wind-forcing (no ice) and constant MLD

$$O_2(t) = O_{2,sat}\left(1 + \Delta O_{2,i}\right)e^{-kt} - \frac{\mathrm{NCP}/h - kO_{2,sat}}{k}\left(1 - e^{-kt}\right) \tag{8}$$

where $\Delta O_{2,i}$ is the initial saturation state and $k$ is the inverse of the ML characteristic gas exchange time ($k = k^{O_2}/h$).

[69] We estimate a regionally typical $k^{O_2}$ based on the ten-year root mean square of daily NCEP/NCAR Reanalysis wind speeds for the Ross Sea region (6.5 m s$^{-1}$) and the piston velocity definition of *Wanninkhof* [1992]. This results in a mean piston velocity of about 2 m d$^{-1}$ at the mean salinity of the Ross Seawater column (34.5) and a sea surface temperature of −1 °C (used to compute the Schmidt number). Using equation (8) we solve for the time when the $O_2$ saturation is within 1% of the steady state value. We find that a 50 m ML starting at $\Delta O_2 \approx -19\%$ requires about 74 days, with zero NCP, and 83 days with NCP = 60 mmol $O_2$ m$^{-2}$ d$^{-1}$ to achieve steady state. Prior to this point, mean daily changes in ML $\Delta O_2$ are about 0.3% per day by gas exchange alone and an additional 0.1% per day from NCP. Based on this simple analysis, we might expect steady state conditions in Ross Sea ML $O_2$ to occur in January, depending on the timing of productivity coordinated with ice dynamics.

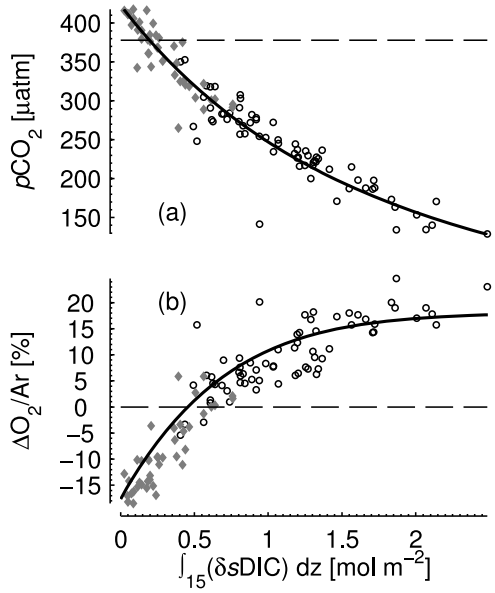


**Figure 13.** (a) Surface $pCO_2$ and (b) $\Delta O_2$/Ar versus depth-integrated $\delta s$DIC above 15 m for C1 (circles) and C2 (diamonds). The lines are the results of a simple 1-box model simulation with constant NCP (40 mmol C m$^{-2}$ d$^{-1}$) and constant wind (4.2 m s$^{-1}$). The model was initialized with deep-water values for *s*DIC, $O_2$, and total alkalinity at concentrations representative of the Ross Sea and run for 90 days. $\Delta O_2$/Ar approaches equilibrium, whereas biological $O_2$ production is balanced by $O_2$ lost to the atmosphere. Since air-sea exchange is more sluggish for $CO_2$ than for $O_2$, $pCO_2$ continues to decline due to biological carbon uptake after $O_2$ concentrations have stabilized. Dashed lines show atmospheric equilibrium concentrations.

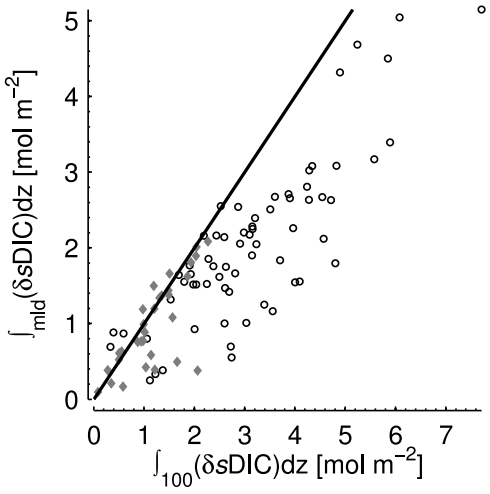


**Figure 14.** Depth-integrated *s*DIC drawdown above the mixed layer depth ($\Delta\sigma_t = 0.05$) versus above 100 m for C1 (circles) and C2 (diamonds). The slope of the black line is 1:1.

[70] The fact that ML $O_2$ in the Ross Sea is significantly undersaturated at the beginning of the season will cause the WPV method to underestimate NCP over much of the growing season. A separate but related issue with the application of this method in the Ross Sea is the fact that rates of NCP are seasonally variable. Testing the WPV method in a 1D box model, we find that when the model conforms to the idealized assumptions implicit in the method, the accuracy of the WPV NCP is dependent on the length of gas exchange history incorporated in the weighting function [*Reuer et al.*, 2007; *Kaiser et al.*, 2005]. The improvement in accuracy beyond about 60 days is not meaningful; however, changes in rates of NCP in the Ross Sea over such a period are quite substantial.

[71] Given the long wind history required to produce accurate NCP estimates, the timescale over which the estimated rates are applicable is poorly constrained, making comparisons with other NCP estimates a challenge [*Reuer et al.*, 2007]. To determine the time period over which NCP variability affects the WPV computation, we used 50 m mixed layer box model, initialized with temperature- and NCP-dependent steady state $O_2$ concentration. We specified a step function change in NCP *n* days prior to "sampling" and represent the degree to which the prior change in NCP is reflected in the WPV NCP result as a weighted average of the two historic NCP rates. The weighting factors in this average quantify the relative contribution of the two historic rates to the reconstructed signal. Repeating this procedure 500 times with stochastic winds (produced from a Weibull distribution fit to ten years of daily Ross Sea wind) yields a robust estimate of the average duration over which NCP signals persist in the ML.

[72] The results of this simple experiment show that (at 0°C) approximately 20% of the information incorporated in an NCP estimate is from the last 5 days, 40% from within the last 10 days, 60% from within the last 20 days, and 90% from within the last 40 days. The memory of the system is slightly temperature dependent (due to the temperature dependence of $O_2$ solubility and Schmidt number), growing longer at the cold conditions characteristic of the Ross Sea. These results indicate that recent variations in NCP and wind are more important to the estimates [*Reuer et al.*, 2007], but the method does incorporate substantial information from the relatively "distant" past. This has significant implications in regions where NCP rates show strong temporal variability. These results are sensitive to the statistical wind distribution driving the model. We did not resolve this distribution seasonally, thus it is likely that the memory changes over the course of the year as the wind regime changes. High wind speeds will reduce the duration that signals persist in the ML.

[73] The bias in the WPV method associated with temporally variable rates of NCP depends on when during the seasonal cycle samples are taken. Given the long memory of mixed layer oxygen, observations taken near the bloom peak in late December/early January are likely to underestimate current NCP rates, presuming that NCP increases through November and December, subsequently declining through February into March. Later in the season, it is possible to generate overestimates of true rates, due the system's memory of higher NCP during the period of peak productivity.

[74] Potential biases in the WPV method notwithstanding, biological oxygen saturation was related to other production metrics during the CORSACS cruises. WPV-NCP during C1 was significantly correlated with mean SeaWiFS-PP over the five days preceding measurement ($R = 0.520, p < 0.001$). This correlation is stronger using the mean NPP for 10 ($R = 0.584$, $p < 0.001$) and 15 days ($R = 0.567$, $p < 0.001$) prior to measurement, then subsequently declines when including additional history (using 5-day increments) in the average, which may reflect $O_2$ dynamics or simply the movement of water through static pixel locations. Based on linear regression analysis of data from C1, the WPV method tends to return values that are about 84 ± 5% ($r^2 = 0.341$) lower than the mean SeaWiFS-PP over the ten days preceding measurement. $\delta s$DIC-derived NCP was about 65% of SeaWiFS-PP on a seasonal timescale, a value consistent with the low temperature export ratios of *Laws et al.* [2000]. Since surface ocean $O_2$ was undersaturated during C2, it is obvious that the WPV method cannot produce accurate estimates of early season NCP and WPV-NCP was not significantly correlated with SeaWiFS-PP during this early season cruise.

[75] A final caveat with using surface data for NCP estimation involves the complexity of vertical structure. As described above, we find that shallow mixing depths cause intense surface drawdown; however, depth integrated drawdown, particularly later in the season, scales approximately linearly with mixing depth and is not well correlated with surface gas distributions. Variability in MLDs likely plays an important role in structuring the distribution of production signals at depth. During both cruises, we find a substantial portion of the integrated NCP signal below the ML (Figure 14 and Table 1); for instance, only about 70% of the NCP signal is above the $\Delta\sigma_t = 0.05$ MLD during the summer and about 85% during spring. These substantial fractions of NCP are, obviously, not reflected in estimates based on ML tracer distributions. The discussion above has been focused on the Ross Sea. It should be emphasized that the WPV method was developed for use in other oceanic regions that conform more closely to the assumptions needed for accurate mass balance calculations. Where the assumptions are

tenable, the method should yield accurate information about ML NCP.

## 4. Summary

[76] Developing accurate measurements of biological rate processes in polar regions, such as the Ross Sea, presents distinct challenges. In particular, temporal rates of change can be large and the weak stratification and geophysical fluid dynamics characteristic of high latitudes create substantial heterogeneity in physical and biological fields at meso- and submesoscales [*Hales and Takahashi*, 2004; *Tortell and Long*, 2009].

[77] The two CORSACS cruises provide insight into two distinct periods of the seasonal cycle and demonstrate substantial interannual variability in productivity dynamics in the Ross Sea. During the summer cruise, the greatest differences in vertical structure and nutrient drawdown intensity resulted from differing ice-melt dynamics across the polynya. Variance in surface gases was decoupled from active biological properties, and reflected the imprint of both seasonally integrated production and ocean stirring. During spring, regions of more intense stratification tended to be proximal to upper ocean fronts, where lateral mechanisms may play an important role in setting early season stratification.

[78] The early season water column is initially undersaturated with respect to $O_2$. The time required for $O_2$ to accumulate in the surface to supersaturated levels, a necessary condition for gas exchange to balance NCP, requires a substantial portion of the growing season. The rate at which steady state is approached is mostly dependent on temperature and wind speed; it is only secondarily dependent on rates of NCP in the Ross Sea. Given the initially undersaturated conditions, high latitude NCP estimates based on gas exchange reconstructions are likely to underestimate true rates over most of the season.

[79] Vertical water column structure has important implications for biogeochemistry in the Ross Sea. In particular, we find that errors in SeaWiFS-PP estimates are correlated with metrics of stratification. Estimation of water column NCP from surface $O_2$ measurements requires knowledge of the vertical depth over which the measured signal is distributed and this can be problematic due to weak stratification and difficulties in diagnosing mixing depths. Our data show that surface drawdown intensity (mol $m^{-3}$) is not necessarily indicative of high depth-integrated drawdown (mol $m^{-2}$), but rather (within the range of our measurements) the latter scales approximately linearly with the depth of mixing. We find a substantial fraction of seasonal NCP below the MLD, as defined by traditional metrics. These factors, and the fact that weak stratification is susceptible to episodic entrainment events, which lower ML $O_2$ concentrations via mixing with deep water below, complicate the interpretation of surface $O_2$ measurements with respect to making inferences regarding NCP. The Ross Sea is a unique environment, however many of these finding are applicable to NCP estimation in oceanic regions and times when waters are originally undersaturated, and the memory of this undersaturation has a significant impact on the mixed layer $O_2$ inventories.

[80] Ultimately, both the rates of carbon fixation over the Ross Sea continental shelf and the fate of this fixed carbon are important to understand the magnitude of the annual Ross Sea carbon sink. Given a potentially substantial lag between production and export, there is a clear need for studies documenting the fate of NCP on the Ross Sea continental shelf. It is clear that resolving tracers in the vertical dimension is necessary. Additionally, a significant limitation of our data is the convolution of space and time, since both physical forcing and biological dynamics continue to evolve as the ship moves along its track. Future studies adopting either a Lagrangian or an Eulerian framework will have distinct advantages.

[81] **Acknowledgments.** This work was supported by the U.S. NSF (OPP-0338350 to R.B.D., OPP-0338157 to W.O.S., and OPP-0338097 to G.R.D.). We thank the captain and crew of the R/V *Nathaniel B. Palmer*. This manuscript benefited from discussions with Kevin Arrigo; we thank him for his thoughtful comments. Additional thanks to Gert van Dijken for providing satellite primary productivity data and code for the PSSM algorithm. The comments of Michael Bender and two anonymous reviewers greatly improved this paper.

## References

Amante, C., and B. W. Eakins (2008), ETOPO1 1 arc-minute global relief model: Procedures, data sources and analysis, Natl. Geophys. Data Cent., NESDIS, NOAA, U.S. Dep. of Commer, Boulder, Colo.

Anderson, L. A., and J. L. Sarmiento (1994), Redfield ratios of remineralization determined by nutrient data analysis, *Global Biogeochem. Cycles*, *8*(1), 65–80, doi:10.1029/93GB03318.

Arrigo, K. R., and C. W. Sullivan (1994), A high resolution bio-optical model of microalgal growth: Tests using sea ice algal community time series data, *Limnol. Oceanogr.*, *39*, 609–631, doi:10.4319/lo.1994.39.3.0609.

Arrigo, K., and G. van Dijken (2003), Impact of iceberg C-19 on Ross Sea primary production, *Geophys. Res. Lett.*, *30*(16), 1836, doi:10.1029/2003GL017721.

Arrigo, K., and G. van Dijken (2004), Annual changes in sea-ice, chlorophyll *a*, and primary production in the Ross Sea, Antarctica, *Deep Sea Res., Part II*, *51*(1–3), 117–138, doi:10.1016/j.dsr2.2003.04.003.

Arrigo, K., D. Robinson, D. Worthen, B. Schieber, and M. Lizotte (1998a), Bio-optical properties of the southwestern Ross Sea, *J. Geophys. Res.*, *103*(C10), 21,683–21,695, doi:10.1029/98JC02157.

Arrigo, K. R., A. M. Weiss, and W. O. Smith Jr. (1998b), Physical forcing of phytoplankton dynamics in the southwestern Ross Sea, *J. Geophys. Res.*, *103*(C1), 1007–1021, doi:10.1029/97JC02326.

Arrigo, K. R., D. H. Robinson, D. L. Worthen, R. B. Dunbar, G. R. DiTullio, M. VanWoert, and M. P. Lizotte (1999), Phytoplankton community structure and the drawdown of nutrients and $CO_2$ in the Southern Ocean, *Science*, *283*(5400), 365–367, doi:10.1126/science.283.5400.365.

Arrigo, K. R., G. R. DiTullio, R. Dunbar, D. H. Robinson, M. L. Van Woert, D. L. Worthen, and M. P. Lizotte (2000), Phytoplankton taxonomic variability in nutrient utilization and primary production in the Ross Sea, *J. Geophys. Res.*, *105*(C4), 8827–8846, doi:10.1029/1998JC000289.

Arrigo, K. R., R. Dunbar, M. P. Lizotte, and D. H. Robinson (2002), Taxon-specific differences in C/P and N/P drawdown for phytoplankton in the Ross Sea, Antarctica, *Geophys. Res. Lett.*, *29*(19), 1938, doi:10.1029/2002GL015277.

Arrigo, K., D. Worthen, and D. Robinson (2003), A coupled ocean-ecosystem model of the Ross Sea: 2. Iron regulation of phytoplankton taxonomic variability and primary production, *J. Geophys. Res.*, *108*(C7), 3231, doi:10.1029/2001JC000856.

Arrigo, K. R., G. van Dijken, and M. Long (2008a), Coastal Southern Ocean: A strong anthropogenic $CO_2$ sink, *Geophys. Res. Lett.*, *35*, L21602, doi:10.1029/2008GL035624.

Arrigo, K. R., G. L. van Dijken, and S. Bushinsky (2008b), Primary production in the Southern Ocean, 1997–2006, *J. Geophys. Res.*, *113*, C08004, doi:10.1029/2007JC004551.

Asper, V., and W. Smith (1999), Particle fluxes during austral spring and summer in the southern Ross Sea, Antarctica, *J. Geophys. Res.*, *104*(C3), 5345–5359, doi:10.1029/1998JC900067.

Azzaro, M., R. La Ferla, and F. Azzaro (2006), Microbial respiration in the aphotic zone of the Ross Sea (Antarctica), *Mar. Chem.*, *99*(1–4), 199–209, doi:10.1016/j.marchem.2005.09.011.

Bates, N. R., D. A. Hansell, C. A. Carlson, and L. I. Gordon (1998), Distribution of $CO_2$ species, estimates of net community production,

and air-sea $CO_2$ exchange in the Ross Sea polynya, *J. Geophys. Res.*, *103*(C2), 2883–2896, doi:10.1029/97JC02473.

Behrenfeld, M. J., and P. G. Falkowski (1997), A consumer's guide to phytoplankton primary productivity models, *Limnol. Oceanogr.*, *42*(7), 1479–1491, doi:10.4319/lo.1997.42.7.1479.

Bender, M., et al. (1987), A comparison of four methods for determining planktonic community production, *Limnol. Oceanogr.*, *32*(5), 1085–1098, doi:10.4319/lo.1987.32.5.1085.

Bender, M., M. Dickson, and J. Orchardo (2000), Net and gross production in the Ross Sea as determined by incubation experiments and dissolved $O_2$ studies, *Deep Sea Res., Part II*, *47*(15–16), 3141–3158, doi:10.1016/S0967-0645(00)00062-X.

Carlson, C., et al. (2000), Stocks and dynamics of dissolved and particulate organic matter in the southern Ross Sea, Antarctica, *Deep Sea Res., Part II*, *47*(15–16), 3201–3225, doi:10.1016/S0967-0645(00)00065-5.

Carr, M., et al. (2006), A comparison of global estimates of marine primary production from ocean color, *Deep Sea Res., Part II*, *53*(5–7), 741–770, doi:10.1016/j.dsr2.2006.01.028.

Cassar, N., M. L. Bender, B. A. Barnett, S. Fan, W. J. Moxim, H. Levy II, and B. Tilbrook (2007), The Southern Ocean biological response to aeolian iron deposition, *Science*, *317*(5841), 1067–1070, doi:10.1126/science.1144602.

Cassar, N., B. Barnett, M. Bender, J. Kaiser, R. Hamme, and B. Tilbrook (2009), Continuous high-frequency dissolved $O_2$/Ar measurements by equilibrator inlet mass spectrometry, *Anal. Chem.*, *81*(5), 1855–1864, doi:10.1021/ac802300u.

Cavalieri, D., P. Gloerson, and J. Zwally (1990), DMSP SSM/I daily polar gridded sea ice concentrations, digital media, edited by J. Maslanik and J. Stroeve, Natl. Snow and Ice Data Cent., Boulder, Colo.

Collier, R., J. Dymond, S. Honjo, S. Manganini, R. Francois, and R. Dunbar (2000), The vertical flux of biogenic and lithogenic material in the Ross Sea: Moored sediment trap observations 1996–1998, *Deep Sea Res., Part II*, *47*(15–16), 3491–3520, doi:10.1016/S0967-0645(00)00076-X.

Craig, A. C., R. B. Nick, W. D. Hugh, and A. H. Dennis (1999), Estimation of bacterial respiration and growth efficiency in the Ross Sea, Antarctica, *Aquat. Microb. Ecol.*, *19*(3), 229–244, doi:10.3354/ame019229.

Craig, H., and T. Hayward (1987), Oxygen supersaturation in the ocean: Biological versus physical contributions, *Science*, *235*(4785), 199–202, doi:10.1126/science.235.4785.199.

Culberson, C. H., and S. Huang (1987), Automated amperometric oxygen titration, *Deep Sea Res., Part A*, *34*(5–6), 875–880, doi:10.1016/0198-0149(87)90042-2.

Dickson, A. G., and C. Goyet (1994), Handbook of methods for the analysis of the various parameters of the carbon dioxide system in sea water, version 2, *Tech. Rep. ORNL/CDIAC-74*, Oak Ridge Natl. Lab., Tenn.

DiTullio, G., and M. Geesey (2002), Photosynthetic pigments in marine algae and bacteria, in *The Encyclopedia of Environmental Microbiology*, vol. 5, edited by G. Bitton, pp. 2453–2470, John Wiley, New York.

DiTullio, G. R., and W. O. Smith Jr. (1996), Spatial patterns in phytoplankton biomass and pigment distribution in the Ross Sea, *J. Geophys. Res.*, *101*, 18,467–18,477, doi:10.1029/96JC00034.

Doney, S. C., D. M. Glover, S. J. McCue, and M. Fuentes (2003), Mesoscale variability of Sea-viewing Wide Field-of-view Sensor (SeaWiFS) satellite ocean color: Global patterns and spatial scales, *J. Geophys. Res.*, *108*(C2), 3024, doi:10.1029/2001JC000843.

Dunbar, R. B. (1984), Sediment trap experiments on the Antarctic continental margin, *Antarct. J. U. S.*, *19*, 70–71.

Dunbar, R. B., A. R. Leventer, and D. A. Mucciarone (1998), Water column sediment fluxes in the Ross Sea, Antarctica: Atmospheric and sea ice forcing, *J. Geophys. Res.*, *103*(C13), 30,741–30,759, doi:10.1029/1998JC900001.

Dunbar, R. B., K. R. Arrigo, M. Lutz, G. R. DiTullio, A. R. Leventer, M. P. Lizotte, M. P. Van Woert, and D. H. Robinson (2003), Non-redfield production and export of marine organic matter: A recurrent part of the annual cycle in the Ross Sea, Antarctica, in *Biogeochemistry of the Ross Sea*, *Antart. Res. Ser.*, vol. 78, edited by G. R. DiTullio and R. Dunbar, pp. 179–195, AGU, Washington, D. C., doi:10.1029/078ARS11.

Dunne, J. P., J. L. Sarmiento, and A. Gnanadesikan (2007), A synthesis of global particle export from the surface ocean and cycling through the ocean interior and on the seafloor, *Global Biogeochem. Cycles*, *21*, GB4006, doi:10.1029/2006GB002907.

Eppley, R. W. (1972), Temperature and phytoplankton growth in the sea, *Fish. Bull.*, *70*(4), 1063–1085.

Falkowski, P., and J. Raven (2007), *Aquatic Photosynthesis*, 2nd ed., Princeton Univ. Press, Princeton, N. J.

Fitzwater, S. E., K. S. Johnson, R. M. Gordon, K. H. Coale, and W. O. Smith Jr. (2000), Trace metal concentrations in the Ross Sea and their relationship with nutrients and phytoplankton growth, *Deep Sea Res., Part II*, *47*, 3159–3179, doi:10.1016/S0967-0645(00)00063-1.

García, H. E., and L. I. Gordon (1992), Oxygen solubility in seawater: Better fitting equations, *Limnol. Oceanogr.*, *37*, 1307–1312, doi:10.4319/lo.1992.37.6.1307.

GLOBALVIEW-CO2 (2008), Cooperative atmospheric data integration project: Carbon dioxide [CD-ROM], NOAA, ESRL, Boulder, Colo. [Available at ftp.cmdl.noaa.gov, Path: ccg/co2/GLOBALVIEW.]

Gordon, L., J. Jennings Jr., A. Ross, and J. Krest (1993), A suggested protocol for continuous flow automated analysis of seawater nutrients (phosphate, nitrate, nitrite and silicic acid) in the WOCE Hydrographic Program and the Joint Global Ocean Fluxes Study, WOCE Operations Manual, *Tech. Rep. 93–1*, Coll. of Oceanic and Atmos. Sci., Oreg. State Univ., Corvallis, Oreg.

Gordon, L. I., L. A. Codispoti, J. C. Jennings, F. J. Millero, J. M. Morrison, and C. Sweeney (2000), Seasonal evolution of hydrographic properties in the Ross Sea, Antarctica, 1996–1997, *Deep Sea Res., Part II*, *47*(15–16), 3095–3117, doi:10.1016/S0967-0645(00)00060-6.

Guéguen, C., and P. D. Tortell (2008), High-resolution measurement of Southern Ocean $CO_2$ and $O_2$/Ar by membrane inlet mass spectrometry, *Mar. Chem.*, *108*(3–4), 184–194, doi:10.1016/j.marchem.2007.11.007.

Hales, B., and T. Takahashi (2004), High-resolution biogeochemical investigation of the Ross Sea, Antarctica, during the AESOPS (U.S. JGOFS) Program, *Global Biogeochem. Cycles*, *18*, GB3006, doi:10.1029/2003GB002165.

Hamme, R., and S. Emerson (2004), The solubility of neon, nitrogen and argon in distilled water and seawater, *Deep Sea Res., Part I*, *51*, 1517–1528, doi:10.1016/j.dsr.2004.06.009.

Hendricks, M., M. Bender, and B. Barnett (2004), Net and gross $O_2$ production in the Southern Ocean from measurements of biological $O_2$ saturation and its triple isotope composition, *Deep Sea Res., Part I*, *51*, 1541–1561, doi:10.1016/j.dsr.2004.06.006.

Hertzog, A., C. Basdevant, and F. Vial (2006), An assessment of ECMWF and NCEP/NCAR reanalyses in the Southern Hemisphere at the end of the pre-satellite era: Results from the EOLE experiment (1971–1972), *Mon. Weather Rev.*, *134*, 3367–3383, doi:10.1175/MWR3256.1.

Hines, K. M., D. H. Bromwich, and G. J. Marshall (2000), Artificial surface pressure trends in the NCEP-NCAR reanalysis over the Southern Ocean and Antarctica, *J. Clim.*, *13*(22), 3940–3952, doi:10.1175/1520-0442(2000)013<3940:ASPTIT>2.0.CO;2.

Ito, T., and M. Follows (2005), Preformed phosphate, soft tissue pump and atmospheric $CO_2$, *J. Mar. Res.*, *63*(4), 813–839, doi:10.1357/0022240054663231.

Juranek, L. W., and P. D. Quay (2005), In vitro and in situ gross primary and net community production in the North Pacific Subtropical Gyre using labeled and natural abundance isotopes of dissolved $O_2$, *Global Biogeochem. Cycles*, *19*, GB3009, doi:10.1029/2004GB002384.

Kaiser, J., M. K. Reuer, B. A. Barnett, and M. L. Bender (2005), Marine productivity estimates from continuous $O_2$/Ar ratio measurments by membrane inlet mass spectrometry, *Geophys. Res. Lett.*, *32*, L19605, doi:10.1029/2005GL023459.

Kalnay, E., et al. (1996), The NCEP-NCAR 40-year reanalysis project, *Bull. Am. Meteorol. Soc.*, *77*(3), 437–471, doi:10.1175/1520-0477(1996)077<0437:TNYRP>2.0.CO;2.

Knap, A., A. Michaels, A. Close, H. Ducklow, and A. Dickson (1994), Protocols for the Joint Global Ocean Flux Study (JGOFS) core measurements, *JGOFS Rep. 19*, JGOFS Int. Proj. Off., Bergen, Norway. (Reprint of the IOC manuals and guides 29.)

Langone, L., R. Dunbar, D. Mucciarone, M. Ravaioli, R. Meloni, and C. A. Nittrouer (2003), Rapid sinking of biogenic material during the late austral summer in the Ross Sea, Antarctica, in *Biogeochemistry of the Ross Sea*, *Antarct. Res. Ser.*, vol. 78, edited by G. R. DiTullio and R. Dunbar, pp. 221–233, AGU, Washington, D. C., doi:10.1029/078ARS14.

Laws, E. A. (1991), Photosynthetic quotients, new production and net community production in the open ocean, *Deep Sea Res.*, *38*(1), 143–167, doi:10.1016/0198-0149(91)90059-O.

Laws, E. A., P. G. Falkowski, J. Smith, O. Walker, H. Ducklow, and J. J. McCarthy (2000), Temperature effects on export production in the open ocean, *Global Biogeochem. Cycles*, *14*, 1231–1246, doi:10.1029/1999GB001229.

Lutz, M. J., K. Caldeira, R. B. Dunbar, and M. J. Behrenfeld (2007), Seasonal rhythms of net primary production and particulate organic carbon flux to depth describe the efficiency of biological pump in the global ocean, *J. Geophys. Res.*, *112*, C10011, doi:10.1029/2006JC003706.

Marinov, I., A. Gnanadesikan, J. R. Toggweiler, and J. L. Sarmiento (2006), The Southern Ocean biogeochemical divide, *Nature*, *441*, 964–967, doi:10.1038/nature04883.

Markus, T. (1999), Results from an ECMWF-SSM/I forced mixed layer model of the Southern Ocean, *J. Geophys. Res.*, *104*(C7), 15,603–15,620, doi:10.1029/1999JC900080.

Markus, T., and B. A. Burns (1995), A method to estimate subpixel-scale coastal polynyas with satellite passive microwave data, *J. Geophys. Res.*, *100*(C3), 4473–4487, doi:10.1029/94JC02278.

Marra, J. (2002), Approaches to the measurement of plankton production, in *Phytoplankton Productivity and Carbon Assimilation in Marine and Freshwater Ecosystems*, edited by P. H. Williams, D. R. Thomas, and C. S. Reynolds, pp. 78–108, Blackwell, Malden, Mass.

Newberger, T. (2004), Underway $pCO_2$ system users manual, technical report, Lamont-Doherty Earth Obs., Columbia University, Palisades, N. Y.

Orsi, A. H., W. M. Smethie Jr., and J. L. Bullister (2002), On the total input of Antarctic waters to the deep ocean: A preliminary estimate from chlorofluorocarbon measurements, *J. Geophys. Res.*, *107*(C8), 3122, doi:10.1029/2001JC000976.

Reuer, M. K., B. A. Barnett, M. L. Bender, P. G. Falkowski, and M. B. Hendricks (2007), New estimates of Southern Ocean biological production rates from $O_2$/Ar ratios and the triple isotope composition of $O_2$, *Deep Sea Res., Part I*, *54*, 951–974, doi:10.1016/j.dsr.2007.02.007.

Reynolds, R., N. Rayner, T. Smith, D. Stokes, and W. Wang (2002), An improved in situ and satellite SST analysis for climate, *J. Clim.*, *15*, 1609–1625, doi:10.1175/1520-0442(2002)015<1609:AIISAS>2.0.CO;2.

Sandrini, S., N. Ait-Ameur, P. Rivaro, S. Massolo, F. Touratier, L. Tositti, and C. Goyet (2007), Anthropogenic carbon distribution in the Ross Sea, Antarctica, *Antarct. Sci.*, *19*(3), 395–407, doi:10.1017/S0954102007000405.

Sarmiento, J. L., T. M. C. Hughes, R. J. Stouffer, and S. Manabe (1998), Simulated response of the ocean carbon cycle to anthropogenic climate warming, *Nature*, *393*, 245–249, doi:10.1038/30455.

Sarmiento, J. L., N. Gruber, M. A. Brzezinski, and J. P. Dunne (2004), High-latitude controls of thermocline nutrients and low latitude biological productivity, *Nature*, *427*, 56–60, doi:10.1038/nature02127.

Sedwick, P. N., G. R. DiTullio, and D. J. Mackey (2000), Iron and manganese in the Ross Sea, Antarctica: Seasonal iron limitation in Antarctic shelf waters, *J. Geophys. Res.*, *105*(C5), 11,321–11,336, doi:10.1029/2000JC000256.

Sedwick, P. N., et al. (2011), Early-season depletion of dissolved iron in the Ross Sea polynya: Implications for iron dynamics on the Antarctic continental shelf, *J. Geophys. Res.*, doi:10.1029/2010JC006553, in press.

Sigman, D. M., and E. A. Boyle (2000), Glacial/interglacial variations in atmospheric carbon dioxide, *Nature*, *407*, 859–869, doi:10.1038/35038000.

Smith, W. O., and R. B. Dunbar (1998), The relationship between new production and vertical flux on the Ross Sea continental shelf, *J. Mar. Syst.*, *17*(1–4), 445–457, doi:10.1016/S0924-7963(98)00057-8.

Smith, W. O., and L. Gordon (1997), Hyperproductivity of the Ross Sea (Antarctica) polynya during austral spring, *Geophys. Res. Lett.*, *24*(3), 233–236, doi:10.1029/96GL03926.

Smith, W. O., J. Marra, M. R. Hiscock, and R. T. Barber (2000), The seasonal cycle of phytoplankton biomass and primary productivity in the Ross Sea, Antarctica, *Deep Sea Res., Part II*, *47*(15–16), 3119–3140, doi:10.1016/S0967-0645(00)00061-8.

Sweeney, C. (2003), The annual cycle of surface water $CO_2$ and $O_2$ in the Ross Sea: A model for gas exchange on the continental shelves of Antarctica, in *Biogeochemistry of the Ross Sea*, *Antarct. Res. Ser.*, vol. 78, edited by G. R. DiTullio and R. Dunbar, pp. 295–312, AGU, Washington, D. C., doi:10.1029/078ARS19.

Sweeney, C., D. A. Hansell, C. A. Carlson, L. A. Codispoti, L. I. Gordon, J. Marra, F. J. Millero, W. O. Smith, and T. Takahashi (2000), Biogeochemical regimes, net community production and carbon export in the Ross Sea, Antarctica, *Deep Sea Res., Part II*, *47*, 3369–3394, doi:10.1016/S0967-0645(00)00072-2.

Tagliabue, A., and K. R. Arrigo (2005), Iron in the Ross Sea: 1. Impact on $CO_2$ fluxes via variation in phytoplankton functional group and non-Redfield stoichiometry, *J. Geophys. Res.*, *110*, C03009, doi:10.1029/2004JC002531.

Tortell, P. (2005), Dissolved gas measurements in oceanic waters made by membrane inlet mass spectrometry, *Limnol. Oceanogr. Methods*, *3*, 24–37, doi:10.4319/lom.2005.3.24.

Tortell, P. D., and M. C. Long (2009), Spatial and temporal variability of biogenic gases during the Southern Ocean spring bloom, *Geophys. Res. Lett.*, *36*, L01603, doi:10.1029/2008GL035819.

Wanninkhof, R. (1992), Relationship between wind speed and gas exchange over the ocean, *J. Geophys. Res.*, *97*(C5), 7373–7382, doi:10.1029/92JC00188.

Weiss, R. F. (1974), Carbon dioxide in seawater: The solubility of an ideal gas, *Mar. Chem.*, *2*, 203–215, doi:10.1016/0304-4203(74)90015-2.

R. B. Dunbar and D. A. Mucciarone, Environmental Earth System Science, Stanford University, 320 Braun Hall, Stanford, CA 94305, USA.

G. R. DiTullio, Grice Marine Laboratory, College of Charleston, 205 Fort Johnson, Charleston, SC 29412, USA.

M. C. Long, National Center for Atmospheric Research, 1850 Table Mesa Dr., Boulder, CO, 80305, USA. (mclong@ucar.edu)

W. O. Smith, Virginia Institute of Marine Science, College of William and Mary, Rt 1208 Greate Rd., Gloucester Point, VA 23062-1346, USA.

P. D. Tortell, Department of Earth and Ocean Sciences and Department of Botany, University of British Columbia, 6270 University Blvd., Vancouver, BC V6T 1Z4, Canada.